Structure of the mirror nuclei ^{9}Be and ^{9}B in a microscopic cluster model

K. Arai[1], Y. Ogawa[2], Y. Suzuki[3], and K. Varga[4]
[1] Graduate School of Science and Technology, Niigata University, Niigata 950-21, Japan
[2] RIKEN, Hirosawa, Wako, Saitama 351-01 Japan
[3] Department of Physics, Niigata University, Niigata 950-21, Japan
[4] Institute of Nuclear Research of the Hungarian Academy of Sciences, Debrecen, P. O. Box 51, H–4001, Hungary

(February 6, 2008)

Abstract

The structure of the mirror nuclei ^{9}Be and ^{9}B is studied in a microscopic $\alpha+\alpha+n$ and $\alpha+\alpha+p$ three-cluster model using a fully antisymmetrized 9-nucleon wave function. The two-nucleon interaction includes central and spin-orbit components together with the Coulomb potential. The ground state of ^{9}Be is obtained accurately with the stochastic variational method, while several particle-unbound states of both ^{9}Be and ^{9}B are investigated with the complex scaling method. The calculation for ^{9}Be supports the recent identification for the existence of two broad states around 6.5 MeV, and predicts the $\frac{3}{2}^-_2$ and $\frac{5}{2}^-_2$ states at about 4.5 MeV and 8 MeV, respectively. The similarity of the calculated spectra of ^{9}Be and ^{9}B enables one to identify unknown spins and parities of the ^{9}B states. Available data on electromagnetic moments and elastic electron scatterings are reproduced very well. The enhancement of the $E1$ transition of the first excited state in ^{9}Be is well accounted for. The calculated density of ^{9}Be is found to reproduce the reaction cross section on a Carbon target. The analysis of the beta decay of ^{9}Li to ^{9}Be clearly shows that the wave function of ^{9}Be must contain a small component that cannot be described by the simple $\alpha+\alpha+n$ model. This small component can be well accounted for by extending a configuration space to include the distortion of the α-particle to $t+p$ and $h+n$ partitions.

PACS number(s): 27.20.+n, 23.20.-g, 23.40.-s, 21.60.Gx

I. INTRODUCTION

There has been a growing interest in the study of neutron-rich nuclei since the advent of radioactive nuclear beams. It was found [1] that some light nuclei near the neutron drip-line exhibit neutron-halo structure or have thick neutron-skin clouds. The halo structure, a new form of the nuclear matter, is characterized by a spatially extended low density distribution around the core part of normal density. It is interesting to know how a nucleus changes its structure with the increase of the number of neutrons and how the binding of the neutrons is attained in such a system. In the very light nuclei the mean field is not stable enough to generate the regular shell structure but, instead, the clustering of the nucleons, especially the α-clustering plays an important role in determining their structure. Because of this the light nuclei show individual features which have strong dependence on the number of nucleons. The Be isotopes are of special interest in this respect because they show some anomalous features which are not easily understood in a simple shell model. Because the ^{8}Be nucleus is known to be a typical cluster state of two α-particles, it is interesting to attempt at describing heavier Be isotopes in a unified framework of two α-particles and extra neutrons. Our basic question is: How well does this picture give us a consistent understanding of the Be isotopes? This question naturally leads us to the application of a multicluster model. A fully microscopic multicluster model utilizes an A-nucleon wave function, incorporating the Pauli principle exactly. It has various applications in the structure study for the halo nuclei [2] and in the nuclear astrophysics [3,4].

The spectrum of ^{9}Be is poorly known. This is probably because all the levels but the ground state are above the $\alpha + \alpha + n$ threshold. Recent experiments [5,6] have, however, isolated the broad level at 6.76 MeV [7] to two states, the $\frac{7}{2}^-$, 6.38 MeV state and the $\frac{9}{2}^+$, 6.76 MeV state.

A few theoretical studies on ^{9}Be have already been done in various models. A projected Hartree-Fock calculation [8] was carried out to study the electromagnetic properties of ^{9}Be. A shell-model calculations in a $(0+1)\hbar\omega$ basis [5,9] gave a reasonable spectrum but predicted too small dipole transition strength for the first excited state. There are several calculations using an $\alpha + \alpha + N$ three-cluster model. Earlier calculations [10,11] emphasized the three-body aspect of ^{9}Be to explain its low-lying spectrum. These treated the α-particle as a structureless particle and considered its compositeness by redefining the potential with the Pauli correction. Recently, this type of macroscopic approach has been extensively applied to the study of ^{9}Be and ^{9}B nuclei [12], by including the $(\alpha\alpha)N$-type arrangement in the calculation. On the other hand, some microscopic cluster-model calculations starting from 9-nucleon wave functions were accomplished in the resonating group method [13] or in the generator coordinate method [14,15,16]. Our microscopic multicluster model has the advantage that the distortion of the constituent clusters, e.g., the α-particle, when needed, can be included in the calculation in a consistent way. An example indicating this necessity will be discussed later in case of the β decay of ^{9}Li to ^{9}Be. The macroscopic model has, however, a difficulty in taking the possibility of the cluster distortion into account.

The calculation of Ref. [13] considered the three channels of ^{8}Be$(0^+)+n$, ^{5}He(g.s.)$+\alpha$, and ^{8}Be$(2^+)+n$ to describe the levels of ^{9}Be. A molecular model was applied in the generator coordinate framework to study the structure of ^{9}Be [14,15]. The calculation of Ref. [16] included only ^{8}Be$+N$ channel, where the motion of the two α-particles in ^{8}Be was described

in a restricted space. The two generator coordinate method calculations gave a reasonable agreement with experiment. There are, however, some noticeable disagreements between the theory and experiment. Both of the macroscopic and microscopic calculations done so far were limited either in taking the Pauli principle into account or in treating the three-body dynamics. Further improvement will be attainable by treating the three-body dynamics more completely.

As the first of the series of studies on the Be isotopes we show in this paper the results of calculation for ^{9}Be in a microscopic $\alpha + \alpha + n$ model. At the same time we consider its mirror nucleus ^{9}B in an $\alpha + \alpha + p$ three-cluster model. One of the main objectives in this paper is to assess the validity of our basic assumption in case of ^{9}Be. This is substantially important for the study on heavier Be isotopes. To this end we carry out an extensive three-cluster model calculation that has no limitations mentioned above, and investigate carefully some important properties of the low-lying states of ^{9}Be, that is, the energy spectrum, the magnetic and quadrupole moments of the $\frac{3}{2}^-$ ground state, and the electron scattering form factors. Of particular interest is the enhancement of the electric dipole transition from the first excited $\frac{1}{2}^+$ state to the ground state [17,18]. This reduced transition probability is nearly as large as the well known one of ^{11}Be. The mechanism of the enhancement in these cases may be related to each other. Another interest is the β decay from ^{9}Li to the low-lying states of ^{9}Be [19]. We will show that this β decay is useful to reveal small components contained in the wave function of ^{9}Be.

The levels of ^{9}B are all particle-unbound and only few of them have spin assignments [7]. There are discussions on the missing $\frac{1}{2}^+$ state from the viewpoint of the Coulomb displacement energy [20,21]. As a mirror nucleus of ^{9}Be, ^{9}B can be described in an $\alpha + \alpha + p$ three-cluster model. A cluster model has a unique advantage that it can describe the asymptotic part of a wave function well and thereby predict the position and width of a resonance. This is a very important ingredient for a detailed structure study of both ^{9}Be and ^{9}B because their states are mostly unbound.

In our approach the total wave function is given as an antisymmetrized product of the internal states of the clusters and the function of the relative motion. The antisymmetrization of all the nucleons is exactly taken into account. Two types of cluster arrangements, $(\alpha\alpha)N$ and $(\alpha N)\alpha$, are combined to include the different correlation between the clusters. The nucleon in the $(\alpha\alpha)N$ arrangement corresponds to moving in a "molecular" orbit around the ^{8}Be=$(\alpha\alpha)$ core. On the contrary, the $(\alpha N)\alpha$ arrangement is suited to describe an "atomic" orbit of the nucleon around the α-particle. This analogy should not, however, be taken so literally particularly when the particles come closer, because the configurations of the two arrangements have considerable overlap. The function of the relative motion is approximated by a linear combination of nodeless harmonic-oscillator functions of different size parameters. Our experience [22,23] shows that the approximation with such functions gives an accurate description up to large distances. To keep the dimension of the basis low, we apply the stochastic variational method (SVM) [23,24,25], in which we set up the "important" basis states stepwise by using an admittance test. This procedure was successfully applied to study the exotic nuclei [2,25,26] and also to few-body systems [23].

The plan of this paper is as follows. In section II we give a brief outline of our formalism. The microscopic three-cluster model is presented in subsection IIA. The scaling methods which we apply to determine the position and width of a resonance state are briefly explained

in subsection IIB. Section III contains the results of calculations. The input parameters are given in subsection IIIA. The relative importance of the arrangements and the angular momentum channels are discussed in subsection IIIB. Energies, radii, magnetic and quadrupole moments, electron scattering form factors are compared with experiment in subsection IIIC. The density distributions and the spectroscopic amplitudes are discussed in subsection IIID. The β decay of ^{9}Li to the states of ^{9}Be is discussed in subsection IIIE. In the last section we summarize the most important conclusions.

II. FORMALISM

A. A microscopic three-cluster model

To describe the system consisting of $\alpha + \alpha + n$ for ^{9}Be or of $\alpha + \alpha + p$ for ^{9}B, we build up a trial function which is a sum over two cluster arrangements μ, $\mu_1 = (\alpha\alpha)N$ and $\mu_2 = (\alpha N)\alpha$, with $N = n$ or p. Each arrangement is associated with a particular set of intercluster Jacobi coordinates $\boldsymbol{\rho}_1^\mu$ and $\boldsymbol{\rho}_2^\mu$. The coordinates $\boldsymbol{\rho}_1^\mu$ and $\boldsymbol{\rho}_2^\mu$ in the arrangement μ_1 are chosen to stand for the relative coordinate of the α-particles and the nucleon coordinate measured from the center-of-mass coordinate of two α's, while, in the arrangement μ_2, they represent the relative distance vector between the nucleon and α and the relative coordinate of another α from the center-of-mass coordinate of the nucleon and α. The arrangement μ_1 is suited to describe the component corresponding to the ^{8}Be+N decomposition at large distances, while the arrangement μ_2 corresponds to the ^{5}He+α decomposition. The total orbital angular momentum L is obtained by coupling the orbital angular momenta $\ell_i \equiv \ell_i^\mu$ belonging to the Jacobi coordinates $\boldsymbol{\rho}_i^\mu$, and then it is coupled with the total spin $S = \frac{1}{2}$ to get the total angular momentum J. See Fig. 1(a). The intrinsic wave function of the α-particle is constructed from a harmonic-oscillator Slater determinant with a fixed size parameter by eliminating the center-of-mass motion. The wave function of the intercluster motion is approximated by a linear combination of nodeless harmonic-oscillator functions (or "Gaussians") of different size parameters:

$$\Gamma_{\ell m}(\nu, \boldsymbol{\rho}) = G_\ell(\nu)\exp(-\nu\rho^2)\mathcal{Y}_{\ell m}(\boldsymbol{\rho}), \tag{1}$$

with

$$G_\ell(\nu) = \left[\frac{2^{2\ell+7/2}\nu^{\ell+3/2}}{\sqrt{\pi}(2\ell+1)!!}\right]^{1/2}, \qquad \mathcal{Y}_{\ell m}(\mathbf{x}) = x^\ell Y_{\ell m}(\hat{\mathbf{x}}). \tag{2}$$

The wave function with the angular momenta $[S,(\ell_1\ell_2)L]JM$ ($S=\frac{1}{2}$) in the arrangement μ can be written as

$$\Psi^\mu_{[S,(\ell_1\ell_2)L]JM} = \sum_K C^\mu_{K,S(\ell_1\ell_2)L}\mathcal{A}\left\{\left[\Phi_S\left[\Gamma_{\ell_1}(\nu^\mu_{k_1},\boldsymbol{\rho}^\mu_1)\Gamma_{\ell_2}(\nu^\mu_{k_2},\boldsymbol{\rho}^\mu_2)\right]_L\right]_{JM}\right\}, \tag{3}$$

where $\nu^\mu_{k_i}$ is the kth size parameter of the ith relative motion in the cluster arrangement μ, $\mathcal{A}$ is the intercluster antisymmetrizer normalized such that the normalization kernel approaches the unit operator in the limit of infinite cluster separation, Φ_{SM_S} is a product of the intrinsic

wave functions of the two α-particles and the nucleon's spin-isospin function and K stands for the set of the indices $\{k_1, k_2\}$ of the size parameters. By using an integral transformation [23], the antisymmetrized product in Eq. (3) can be rewritten as a linear combination of Slater determinants of Gaussian wave-packet single-particle functions. The matrix elements between Slater determinants of these nonorthogonal single-particle states are easily evaluated and can be expressed in a closed analytical form.

The variational trial function is a combination of different arrangements and intercluster angular momenta:

$$\Psi_{JM} = \sum_{(\ell_1\ell_2)L} \left\{ \Psi^{\mu_1}_{[S,(\ell_1\ell_2)L]JM} + \Psi^{\mu_2}_{[S,(\ell_1\ell_2)L]JM} \right\}. \tag{4}$$

It is noted that our wave function is fully antisymmetrized, free from the spurious center-of-mass motion (actually the total center-of-mass motion is eliminated) and has a good total angular momentum and parity. Our calculation is the so-called "variation after projection" type.

The partial waves in a given cluster arrangement form a complete set of states and the different Jacobi coordinate systems are, therefore, equivalent in principle. One might thus think that we only need to choose a particular arrangement, μ_1 or μ_2, and to decompose the wave function into a complete set of partial waves in this arrangement, and that the inclusion of both the arrangements implied in Eq. (4) would be redundant. Our experience [22] shows, however, that the convergence of energy in a fixed arrangement is rather slow. The reason is that the components $\Psi^{\mu_1}_{[S,(\ell_1\ell_2)L]JM}$ and $\Psi^{\mu_2}_{[S,(\ell_1'\ell_2')L']JM}$ in the arrangements μ_1 and μ_2 are rather different, especially, at large distances and that any component $\Psi^{\mu_1}_{[S,(\ell_1\ell_2)L]JM}$ can only be represented by an infinite sum in terms of the arrangement μ_2. Moreover, the inclusion of high partial waves in the calculation is quite expensive. Our favorite choice is, therefore, to (1) decompose the wave function into partial waves in a given arrangement, (2) truncate the higher partial waves, and (3) complete the wave function by the inclusion of low partial waves of different arrangements.

The arrangements and the angular momenta combined with the size parameters in the expansion make the dimension of the basis large. These basis functions are, however, nonorthogonal to each other and not all of them are equally important. In a previous paper [25] we tested different methods to select the parameters $\nu^{\mu}_{k_i}$ that span most adequately the state space, while the dimension of the basis is kept feasible. The most efficient procedure found is the stochastic selection [22,23]: We generate size parameter sets by a random choice from a region which is physically important. The parameter sets that satisfy an admittance condition are chosen to generate basis states. The calculation was repeated several times to check the convergence. The dimension for the ^{9}Be ground state is around 90.

B. The scaling method for resonances

Except for the ground state of ^{9}Be, all the states of ^{9}Be and ^{9}B are above the three-body threshold. The $\frac{1}{2}^+$, 1.68 MeV state of ^{9}Be lies just 111 keV above the threshold, but has a width of 217$\pm$10 keV. The $\frac{5}{2}^-$, 2.43 MeV state has a narrow width. The widths of other

states of isospin $\frac{1}{2}$ range from several hundreds keV to about 1 MeV. The states of ^{9}B have generally wider widths than the corresponding states of ^{9}Be.

Resonances are associated with complex eigenvalues of the time-independent Schrödinger equation. It is not trivial to calculate the energy and the width of a resonance state for a complex system. Several methods have been developed to obtain these complex eigenvalues using square integrable functions. The most well-known methods are the complex scaling [27] and the stabilization [28] methods.

The complex scaling method uses the unitary transformation which dilates the internal coordinates of the system according to $x \to xe^{i\theta}$, making the resonant wave functions square integrable. The eigenvalues that are associated with metastable resonance states appear as such complex eigenvalues that are independent of the scaling angle θ, when it is larger than a critical angle, and the eigenvalues that are associated with nonresonant continuum states appear as complex eigenvalues which are dependent on the scaling angle [27]. One can expand the eigenfunctions of the complex scaled Hamiltonian in terms of square integrable basis functions as we did for bound states. The variation of the energy functional with respect to the trial function, however, yields a stationary rather than a minimum principle. Therefore, the stochastic basis selection procedure cannot be applied here, but instead, we will work on a basis with fixed nonlinear parameters.

The stabilization method [28] utilizes the discrete states calculated in a box of large size. The stabilization method can be combined with the stochastic variational method. In this case we select the basis parameters from a confined interval.

These methods have been widely applied for two- and three-body resonances in atomic physics. Recently, nuclear physicists have also began to use the complex scaling method as a useful tool to locate two- [29] and three-body [30] resonances of nuclear systems.

Due to the complexity of the problem both methods require extreme numerical accuracy. To be on the safe side, we used these methods only when they are certainly able to give reliable results. That is, we used the stabilization method for narrow resonances, and calculated only the resonance energy because the calculation of the width would require an excessively large computational burden. For these quasibound states the stabilized wave functions can directly be used to calculate the matrix element of a physical operator because they are real. To locate wider resonances we used the complex scaling method. In this case we calculated both the width and the position.

We have found that the energy of the narrow $\frac{5}{2}^-$ state can well be obtained by diagonalizing the Hamiltonian in a sufficiently large basis of Eq. (3). The resonance energy remains rather stable against the change of the basis set within a reasonable range. The wave function obtained in this way is used to calculate the electromagnetic transition rates. It is very difficult to do better than this because enclosing the wave function in a box as required by the stabilization method is not trivial for the three-body system.

To apply the complex scaling method to the present case, we define the transformation $U(\theta)$ which acts on the function of the intercluster Jacobi coordinates, $\boldsymbol{\rho}_1^\mu$ and $\boldsymbol{\rho}_2^\mu$,

$$U(\theta) f(\boldsymbol{\rho}_1^\mu, \boldsymbol{\rho}_2^\mu) = \mathrm{e}^{3i\theta/2} f(\boldsymbol{\rho}_1^\mu \, \mathrm{e}^{i\theta}, \boldsymbol{\rho}_1^\mu \, \mathrm{e}^{i\theta}). \tag{5}$$

The eigenvalue problem of the transformed Hamiltonian $H_\theta = U(\theta) H U(\theta)^{-1}$ is solved for each θ value. A resonance state corresponds to an square integrable solution of the transformed Hamiltonian and may be described as in Eq. (4). When the basis function of Eq. (3)

is employed, the operation $U(\theta)^{-1}$ on the relative motion function is equivalent to multiplying the size parameters, $\nu^{\mu}_{k_1}$ and $\nu^{\mu}_{k_2}$, by $\mathrm{e}^{-2i\theta}$. The energy E_R and the width Γ_R of a resonance are obtained as the real and imaginary parts of a complex eigenvalue, $E_\theta = E_R - \frac{1}{2}i\Gamma_R$, of H_θ, which remains unchanged for arbitrary values of θ within an appropriate range.

III. RESULTS

A. Input parameters

The internal state of the α-particle was approximated by 0s harmonic-oscillator Slater determinant wave function of a size parameter ν=$m\omega/2\hbar$. The value of ν was chosen to be 0.26 fm^{-2} to reproduce the experimental charge radius of the α-particle. The results are insensitive to the choice of the size parameter within a reasonable limit.

We used Minnesota nucleon-nucleon interaction [31], which is a sum of central and spin-orbit potentials of Gaussian form. The Coulomb potential was included. The strength of the spin-orbit force was taken from the set IV of Reichstein and Tang, which gives a good fit to N+α phase shifts. The central part of the Minnesota potential contains an exchange-mixture parameter u. The potential with u=1 corresponds to a Serber type mixture. Decreasing the value of u from unity implies increasing repulsion in odd partial waves, while keeping the strength of even partial waves unchanged. It was set to $u = 0.94$ in order to reproduce the ground state energy of ^{9}Be. The value of $u = 0.94$ is very close to the value (0.95) which is needed to well describe the $\alpha + \alpha$ scattering in the resonating group method [31]. Thus our choice should give a realistic interaction between the α-particles. The value of $u = 0.94$ is, however, slightly smaller than the value of 0.97 recommended for the description of $N + \alpha$ scattering. By fixing the u and ν parameters as described above, the model contains no free parameter. No change of the potential parameters was made between ^{9}Be and ^{9}B.

B. Cluster arrangements and angular momentum channels

In our model the total spin is uniquely given by S=$\frac{1}{2}$ so that the total orbital angular momentum can take either $L = J - \frac{1}{2}$ or $L = J + \frac{1}{2}$. Let us show that both values of L are needed by taking an example of the magnetic moment of ^{9}Be. Quite probably (and this will be confirmed later) the orbital motion of the protons gives a moderate contribution to the magnetic moment of ^{9}Be and only the spin part needs to be considered to get a reasonable estimate of the magnetic moment. The magnetic moment is then approximated by (J=$\frac{3}{2}$, $L = 1$ and $L = 2$)

$$\begin{aligned}\mu = \langle \Psi_{JJ}|\mu_z|\Psi_{JJ}\rangle &= g_s(n)\sum_L c_L^2 \left(\sum_{M_S M_L} \langle SM_S LM_L|JJ\rangle^2 M_S \right) \\ &= g_s(n)\sum_L c_L^2 \left(\frac{[J(J+1)+S(S+1)-L(L+1)]J}{2J(J+1)} \right), \end{aligned} \tag{6}$$

where $g_s(n) = -3.826$ is the spin g-factor of the neutron in units of nuclear magneton and c_L is the amplitude of the total orbital angular momentum L in the ground state wave function.

If the ground state is purely of L=1, then the magnetic moment becomes $-1.913\ \mu_N$, which is in disagreement with the observed value of $\mu_{\rm exp} = -1.1778\ \mu_N$. An L =2 component of about 20 % admixture is needed to reproduce the observed value. We will see later that the potential chosen gives just the needed admixture. It is instructive to note that the magnetic moment for pure L=1 case is equal to the Schmidt value of the single $p_{3/2}$ neutron.

Table I lists a set of arrangements and angular momenta used in the present calculation. We did several pilot calculations to know the relative importance of the arrangements and the angular momentum channels. When all the nine sets of Table I are used for the $\frac{3}{2}^-$ ground state, the energy from the $\alpha + \alpha + n$ threshold is obtained as -1.431 MeV and the root mean square (rms) radius of point nucleon is 2.50 fm. Let us call this a full calculation. When we exclude three sets belonging to the arrangement $\mu_2 = (\alpha N)\alpha$ with $\ell_1 = 0$ or 2, both energy and radius hardly change from the result of the full calculation; the overlap of the approximate wave function with the full wave function is 0.9995. This result is physically acceptable because the p wave is of prime importance for the interaction between the neutron and the α-particle. If we further exclude three sets belonging to the μ_2 arrangement with $\ell_1 = 1$, then the energy increases to -0.32 MeV and the radius increases to 2.57 fm. This suggests that the arrangement $\mu_1 = (\alpha\alpha)N$ (^{8}Be+n-type configuration) alone is imperfect to describe the ground state even though the s and d waves are taken into account for the motion of the two α-particles. This consideration leads us to the remark that the calculations of Refs. [12,16] using only the ^{8}Be+N channel should be accepted with some reservations. On the other hand, if we exclude three sets belonging to the μ_1 arrangement, then the result is very close to the full calculation; the energy loss is merely 34 keV and the overlap of the wave functions is 0.9991. We can thus conclude that the ^{5}He+α-type configuration with ℓ_1=1 constitutes a very good approximation to the ground state wave function. As is seen from Table I, the angular momentum in the μ_2 arrangement is restricted to $\ell_1 = 1$ for other states.

For resonance states, particularly for high spin resonances the inclusion of high partial waves becomes important to obtain stable resonance parameters in the complex scaling method. The complex eigenvalue of the rotated Hamiltonian H_θ is obtained by using the basis function of Eq. (3). The size parameters of the basis function are not selected randomly but are chosen as $\nu_k^\mu = \nu_0 p^{k-1}$ ($k = 1, ..., K$). The values of ν_0 and K are varied for each resonance to get stable values for its energy and width. The adopted value of K is about 10 in the present calculation. The basis dimension used to diagonalize the rotated Hamiltonian is K^2 times the number of the sets listed in Table I. Figure 2 displays an example of the complex scaled spectra of ^{9}Be for $J^\pi = \frac{3}{2}^-$ and $\frac{7}{2}^-$. One can see, besides the discretized points corresponding to the three-body continuum, those points which lie on straight lines starting from the positions of the resonances of the subsystems.

C. Energy spectrum and electromagnetic properties

The calculated spectra of ^{9}Be and ^{9}B are compared with experiment in Fig. 3. The theoretical level sequence in ^{9}Be has a good correspondence with the observed spectrum. The second $\frac{3}{2}^-$ resonance is obtained at 4.3 MeV excitation energy. The other calculations [14,15,16] also predict the $\frac{3}{2}^-_2$ state. Although no such state is cited in Ref. [7], the calculated

resonance may correspond to the state at 5.59 MeV mentioned in Ref. [6]. We get two broad overlapping resonances with $\frac{7}{2}^-$ and $\frac{9}{2}^+$ at about 6.5 MeV. This agrees with the conclusion of the recent experiments [5,6]. We could not find a resonance with $\frac{1}{2}^-$ around 8 MeV excitation energy in accordance with Refs. [5,6], although such a state is parenthetically quoted in Ref. [7]. Instead of this a $\frac{5}{2}^-$ resonance is obtained at 7.9 MeV, which agrees with the result of Refs. [14,15]. The spectrum of ^{9}B is less known experimentally compared to that of ^{9}Be. The calculated spectrum is similar to the one of ^{9}Be. We can predict the energy and the width of several resonances in ^{9}B with the same accuracy as the case of ^{9}Be. For example, our calculation predicts a missing $\frac{1}{2}^-$ state at 2.43 MeV, which is in agreement with the result of a recent ^{9}Be(p,n) reaction [32] that located the $\frac{1}{2}^-$ state at 2.83 MeV. Although no definitive spin assignment is made to the state at 2.788 MeV excitation energy [7], our calculation supports a $\frac{5}{2}^+$ assignment rather than $\frac{3}{2}^+$.

Table II lists the energies and the widths of the unbound states calculated by the complex scaling method. The energies of the $\frac{5}{2}^-$ states of both ^{9}Be and ^{9}B are in good agreement with experiment. Their widths, though extremely narrow, are reasonably reproduced; the calculated width of ^{9}Be is about 2 times larger than the observed value, while the width of ^{9}B is about a half of the experiment. The calculation reproduces the widths of other states within a factor of 2. Our result is in better agreement with experiment than the calculation of Ref. [16].

There has been considerable effort to determine the location of the $\frac{1}{2}^+$ state from the point of view of a Thomas-Ehrman shift [33]. We applied the complex scaling method to find a resonance with $J^\pi = \frac{1}{2}^+$ by including the arrangements and the angular momentum channels listed in Table I. The present calculation could not identify such a stable complex eigenvalue that can be interpreted as a resonance. To estimate the $E1$ transition strength, we increase the value of u to make the $\frac{1}{2}^+$ state particle-bound.

The electromagnetic moments and the rms radii of proton, neutron, and nucleon, assuming pointlike nucleons, are included in Table III. Bare operators are used in the calculation. The charge radius of ^{9}Be with the effect of the proton's finite size becomes 2.54 fm and fits the experimental value of 2.519 ± 0.012 fm [7]. The rms radius of neutron is larger than that of proton by 0.2 fm. Both the magnetic and the quadrupole moments of ^{9}Be are reproduced very well. As was stated in subsection IIIB, the contribution of the proton's orbital motion to the magnetic moment is rather small ($0.28\ \mu_N$) and the contribution of the spin part, $-1.45\,\mu_N$, corresponds to 15.1 % admixture of the L =2 component. The $M1$ and $E2$ transition probabilities of the $\frac{5}{2}^-$ state to the ground state are also well reproduced. The strong $E1$ transition of the $\frac{1}{2}^+$ state is in reasonable agreement with experiment. The $E1$ transition strength depends on the description of the tail part of the wave function. With $u = 1.0$ the energy of the $\frac{1}{2}^+$ state changes to 593 keV below the threshold and the $B(E1)$ value becomes 0.24 W.u. in good agreement with experiment. With $u = 0.98$ the energy goes up to 206 keV below the threshold and the exterior part of the wave function that does not contribute to the transition grows, thereby reducing the $B(E1)$ value to 0.18 W.u. To our best knowledge, this is the first theoretical calculation which has been able to reproduce the $E1$ transition probability in a consistent way. Reference [18] argues that the experimental $E1$ strength is enhanced to 0.38±0.07 W.u. if the unbound nature of the state is taken into account.

Table III includes the results of other models. The μ and Q moments of the shell model were determined by using an effective interaction which was chosen to reproduce both energies and static moments of $0p$-shell nuclei [9]. These values are rather close to those of Cohen-Kurath (8-16) POT calculation [34,5]. A shell-model calculation of $(0+1)\hbar\omega$ model space [9] cannot account for the enhancement of the $B(E2)$ transition; with the effective charge of $0.35e$ it gives about one third of the experimental value. The $E1$ transition probability of the lowest $\frac{1}{2}^+$ state to the ground state was predicted to be only 0.03 W.u. [9]. Another shell-model calculation in a similar basis [5] reproduces reasonably the $B(E2)$ value by using a large effective charge for neutron, but again gives a very small $B(E1)$ value. Although the calculation of Ref. [16] using only ^{8}Be+n channel gives a reasonable agreement with experiment, we have already pointed out that the ^{5}He+α type configuration leads to further improvement. A similar remark applies to the calculation of Ref. [12], which indicates that the charge radius and the quadrupole moment are considerably smaller than experiment.

Further test of the wave function of the ^{9}Be ground state is performed by the electron scattering data [35]. The longitudinal electron scattering form factor is calculated in a first-order plane wave Born approximation through

$$|F_L(q)|^2 = \frac{4\pi}{Z^2(2J_i+1)} \sum_\ell |\langle \Psi_{J_f} \| \hat{M}^{\rm coul}_\ell(q) \| \Psi_{J_i} \rangle|^2, \tag{7}$$

where Ze is the charge of the nucleus and the reduced matrix element of the operator $T^k_\kappa(q)$ is defined by

$$\langle JM|T^k_\kappa|J'M'\rangle = \frac{(-1)^{2k}}{\sqrt{2J+1}} \langle J'M'k\kappa|JM\rangle \langle J\|T^k\|J'\rangle. \tag{8}$$

The charge density multipole operator $\hat{M}^{\rm coul}_{\ell m}(q)$ which occurs in the form factor is given as a function of momentum transfer q from the charge density operator

$$\hat{M}^{\rm coul}_{\ell m}(q) = \int j_\ell(qr) Y_{\ell m}(\hat{\mathbf{r}}) \sum_{i=1}^{A} \frac{1-\tau_{3_i}}{2} \delta(\mathbf{r}_i - \mathbf{R}_{\rm cm} - \mathbf{r}) d\mathbf{r}, \tag{9}$$

where $\mathbf{r}_i$ is the nucleon coordinate and $\mathbf{R}_{\rm cm}$ is the total center-of-mass coordinate. Note that our wave function contains no center-of-mass motion. Figure 4 compares the calculated charge form factor with the experiment [36,37,38]. The correction for the finite proton size is taken into account by multiplying the form factor with the proton's form factor used in Ref. [39]. Both monopole (C0) and quadrupole (C2) terms contribute to the charge form factor. No effort has so far been made to separate those contributions experimentally. Polarized electrons and targets will be needed to do such experiments. The agreement between theory and experiment is good. This is perhaps not very surprising because the present model reproduces both charge radius and quadrupole moment accurately. It is clear that the quadrupole deformation of the charge density is important at higher q^2 values. The deformation of the proton and neutron density distributions will be discussed in the next subsection.

The transverse electron scattering form factor gives information on the nuclear current density. It is calculated from the expression

$$|F_T(q)|^2 = \frac{4\pi}{Z^2(2J_i+1)} \sum_\ell \Big\{ |\langle \Psi_{J_f} \| \hat{T}^{\rm el}_\ell(q) \| \Psi_{J_i} \rangle|^2 + |\langle \Psi_{J_f} \| \hat{T}^{\rm mag}_\ell(q) \| \Psi_{J_i} \rangle|^2 \Big\}. \tag{10}$$

The symmetry consideration on parity and time reversal shows that the elastic form factor receives no contribution of the transverse electric multipoles of the current density $\hat{\boldsymbol{j}}(\mathbf{r})$. The transverse magnetic multipoles are defined by

$$\hat{T}^{\rm mag}_{\ell m}(q) = \int j_\ell(qr) \boldsymbol{Y}^m_{\ell\ell 1}(\hat{\mathbf{r}}) \cdot \hat{\boldsymbol{j}}(\mathbf{r}) d\mathbf{r}. \tag{11}$$

Here the vector spherical harmonics are defined with unit vector $\mathbf{e}$ as

$$\boldsymbol{Y}^m_{\ell'\ell 1}(\hat{\mathbf{r}}) = [Y_\ell(\hat{\mathbf{r}})\mathbf{e}]^{\ell'}_m \tag{12}$$

and the current density consists of the convection and magnetization currents:

$$\begin{aligned} \hat{\boldsymbol{j}}(\mathbf{r}) = & \frac{1}{2mc} \sum_{i=1}^A \frac{1-\tau_{3_i}}{2} \Big\{ \mathbf{p}_i \delta(\mathbf{r}_i - \mathbf{R}_{\rm cm} - \mathbf{r}) + \delta(\mathbf{r}_i - \mathbf{R}_{\rm cm} - \mathbf{r}) \mathbf{p}_i \Big\} \\ & + \nabla \times \left(\frac{\hbar}{2mc} \sum_{i=1}^A \mu_i \delta(\mathbf{r}_i - \mathbf{R}_{\rm cm} - \mathbf{r}) \boldsymbol{\sigma}_i \right). \end{aligned} \tag{13}$$

Here $\mathbf{p}_i$ is the momentum of the nucleon in the center-of-mass system and μ_i is the magnetic moment of the nucleon in units of nuclear magneton. Figure 5 compares the calculated transverse form factor with the data of Refs. [40,41]. Both $M1$ and $M3$ contributions are important to get a satisfactory reproduction of experiment. Shell-model calculations [5] needed a quenching factor of about 0.7 for the transverse form factors, while no quenching is needed in our model. We can conclude that the ground-state wave function of the present model reproduces consistently all the electromagnetic properties of ^{9}Be.

D. Density distributions and spectroscopic amplitudes

The proton and the neutron density distributions, defined by

$$\rho(\mathbf{r}) = \Big\langle \Psi_{JJ} \Big| \sum_{i=1}^A \delta(\mathbf{r}_i - \mathbf{R}_{\rm cm} - \mathbf{r}) P_i \Big| \Psi_{JJ} \Big\rangle = \rho_0(r) + \sum_{\ell \neq 0} \rho_\ell(r) Y_{\ell 0}(\hat{\mathbf{r}}), \tag{14}$$

(where P_i projects out the protons or neutrons) are also determined. For the ground state of ^{9}Be we have monopole and quadrupole($\ell = 2$) densities. The density distributions, $\rho_0(r)$ and $\rho_2(r)$, are shown in Figs. 6(a) and 6(b). They are related to the rms radius and the quadrupole moment as below:

$$\langle r^2 \rangle = \frac{4\pi}{Z} \int_0^\infty \rho_0(r) r^4 dr, \tag{15}$$

$$Q = (\frac{16\pi}{5})^{1/2} \int_0^\infty \rho_2(r) r^4 dr. \tag{16}$$

An analogous relation can be defined for the neutron case. The quadrupole moment becomes 5.13 fm^2 for the proton and 3.86 fm^2 for the neutron. The fact that the neutron quadrupole

moment is smaller than the proton quadrupole moment is understood by noting that the single neutron cluster moves between the two α-particles for the most of time and thus makes the neutron density less deformed.

The 2.43 MeV, $\frac{5}{2}^-$ and 6.38 MeV, $\frac{7}{2}^-$ states of ^{9}Be together with the ground state approximately follow a $J(J+1)$ rule and can be considered to form a rotational band with K=$\frac{3}{2}$ [5,6]. ¿From the experimental quadrupole moment of the ground state, the intrinsic quadrupole moment Q_0 of the band is estimated as 26.5 fm^2 by using the relation $Q = \frac{J(2J-1)}{(J+1)(2J+3)}Q_0 = \frac{1}{5}Q_0$ [42]. The $E2$ transition probability within the band is related, in the collective model, to the Q_0 value by

$$B(E2; KJ_1 \rightarrow KJ_2) = \frac{5}{16\pi}e^2Q_0^2\langle J_1K20|J_2K\rangle^2, \tag{17}$$

which predicts 23.9 e^2fm^4 and 9.98 e^2fm^4 for the $\frac{5}{2}^- \rightarrow \frac{3}{2}^-$ and $\frac{7}{2}^- \rightarrow \frac{3}{2}^-$ transitions, respectively. The corresponding experimental values are 27.1$\pm$2.0 e^2fm^4 and 7.0$\pm$3.0 e^2fm^4 [7]. Since the collective model prediction agrees reasonably well with experiment, it may be possible to extract the intrinsic deformation parameter β_0 by using the relation $\beta_0 = \sqrt{\frac{\pi}{5}}\frac{Q_0}{Z\langle r^2\rangle}$. Our theory gives β_0=0.89, which is close to the empirical deformation parameters of neighbouring nuclei, e.g., β_0 $\sim$1.13 for ^{10}Be and β_0 $\sim$0.82 for ^{10}C, while the corresponding Q_0 values are 22.9 fm^2 and 25.0 fm^2, respectively [43]. The deformation parameter β associated with the density of Eq. (14) is estimated by assuming that it can be approximated by $\rho_s(r/(1-\frac{1}{4\pi}\beta^2+\beta Y_{20}(\hat{\mathbf{r}}))$ from a spherical shape $\rho_s(r)$. The extracted value of β is close to 1/5 of the β_0 value as expected by the collective model.

The monopole densities of the protons and the neutrons may be used to calculate the total reaction cross section at high energies. It is given, in the Glauber theory [44], as

$$\sigma_R = \int [1 - \exp\{-2\mathrm{Im}\chi(\mathbf{b})\}]d\mathbf{b}, \tag{18}$$

where $\mathbf{b}$ is the impact parameter and the phase shift function, χ, is related to the densities of the target and the projectile through the thickness function, $T(\mathbf{s}) = \int \rho(\mathbf{s}, z)dz$, by

$$i\chi(\mathbf{b}) = -\iint T_P(\mathbf{s})T_T(\mathbf{t})\Gamma(\mathbf{b}+\mathbf{s}-\mathbf{t})d\mathbf{s}d\mathbf{t}. \tag{19}$$

Here Γ is the profile function for the NN scattering. The monopole densities of the proton and the neutron were used to construct the density of ^{9}Be. The σ_R value of ^{9}Be for a Carbon target at 800 MeV/nucleon is calculated to be 850 mb with the parametrization of the profile function used in Ref. [45]. The interaction cross section measured by Tanihata *et al.* [1] is not exactly the same as but approximately equal to the reaction cross section. Their value is 806$\pm$9 mb, which is in a fair agreement with theory. The reaction cross section of ^{9}Be on a Cu target was measured by Saint-Laurent *et al.* [46] at about 45 MeV/nucleon. They extracted the reduced strong absorption radius, $r_0 \sim 1.13$ fm, for ^{9}Be by fitting their measured cross sections to the formula by Kox *et al* [47]. This formula predicts σ_R = 825$\pm$20 mb for the ^{9}Be+^{12}C system at relativistic energies as listed in Table III. We again confirm that our density is reliable enough to reproduce the experiment.

We showed in the previous subsection that the enhancement of the $E1$ transition of the first excited state in ^{9}Be is reproduced well. To understand this we note that the $E1$ operator

is recast to $\frac{NZ}{A}e\sqrt{\frac{3}{4\pi}}(\mathbf{R}_Z - \mathbf{R}_N)$, where $\mathbf{R}_Z$ and $\mathbf{R}_N$ are the center-of-mass coordinates of the protons and the neutrons, respectively. The enhancement of the transition should be therefore related to the excitation of the corresponding motion in the excited state. In the $\alpha + \alpha + n$ model the $E1$ excitation is caused by the valence neutron. Figure 7 compares the monopole density of the $\frac{1}{2}^+$ state obtained with $u = 1.0$ with that of the ground state. The proton density becomes smaller near the center but reaches up to larger distances, indicating the increase in the mean distance between the two α-particles. The neutron density shows a substantial decrease at 1$\sim$2 fm and a significant increase beyond 3 fm. The proton and neutron rms radii increased from 2.39 to 2.94 fm and from 2.58 to 5.59 fm, respectively. Though the increase of the proton size is moderate, that of the neutron size is dramatic. The picture emerging from this analysis is the following: The valence neutron in the ground state is mostly confined between the two α-particles but, in the excited $\frac{1}{2}^+$ state, moves around them in a spatially wider region. It is easy to understand that the large $E1$ transition strength has naturally come out from the structure change of the underlying states.

Another interesting quantity that helps to reveal information on the wave function is the spectroscopic amplitude which, in the angular momentum projected basis, is defined by

$$g^{\mu}_{(\ell_1\ell_2)L}(r,R) = \frac{1}{r^2R^2}\langle \mathcal{A}\left\{\left[\Phi_S\left[Y_{\ell_1}(\hat{\boldsymbol{\rho}}^{\mu}_1)Y_{\ell_2}(\hat{\boldsymbol{\rho}}^{\mu}_2)\right]_L\right]_{JM}\delta(\rho^{\mu}_1 - r)\delta(\rho^{\mu}_2 - R)\right\}|\Psi_{JM}\rangle. \qquad (20)$$

Figures 8(a), 8(b), and 8(c) display the spectroscopic amplitudes of the ground state of ^{9}Be for some channels of the arrangement $\mu_1 = (\alpha\alpha)n$, letting r and R represent the distances of the two α-particles and of the neutron from their center-of-mass, respectively. Some remarkable features are that all the amplitudes have a peak at $r \sim 3.2$ fm and $R \sim 2.3$ fm and R-independent nodes at $r = 1$ fm (for the s wave between α's) and $r = 2$ fm (for the s and d waves). These characteristics are understood by the microscopic α-α cluster-model analysis for ^{8}Be. The appearance of the nodes is understood in relation to the existence of the Pauli-forbidden states [48]. The norm of the amplitude, which is called the spectroscopic factor, becomes 1.03, 0.77, and 0.32 corresponding to three channels shown in Fig. 8. We note that the norm is different from the so-called amount of clustering. The amplitudes corresponding to the arrangement $\mu_2 = (\alpha n)\alpha$ are plotted in Fig. 9, where r is now the distance between n and α and R the distance between their center-of-mass and α. The nodes appear also in this case but their positions alter particularly at large r. This is due to the fact that R is approximately equal to the α-α distance at small r but deviates largely from it with increasing r. The spectroscopic factor is 0.84 and 0.61, respectively.

E. Beta decay of the ^{9}Li ground state to ^{9}Be

Because the ground state and the $\frac{5}{2}^-$, 2.43 MeV state are described well by the present model, the β decay of the ^{9}Li ground state to these states is expected to further test the accuracy of their wave functions or an available wave function of ^{9}Li. The experimental value of $\log ft$ for the β decay to the ^{9}Be ground state is about 5.31 [7,19], indicating that the β-decay matrix element is fairly suppressed despite the allowed transition. The weak

β decay is ascribed to the fact that the spatial symmetry of the main component of ^{9}Be is different from that of ^{9}Li [34]. The Gamow-Teller (GT) matrix element,

$$M_{GT}(i \to f) = \Big\langle \Psi_{J_f}(^9\mathrm{Be}) \,\Big\|\, \sum_{k=1}^{9} t_-(k)\boldsymbol{\sigma}(k) \,\Big\|\, \Psi_{J_i}(^9\mathrm{Li}) \Big\rangle, \tag{21}$$

to any state of ^{9}Be, if it is described by the $\alpha+\alpha+n$ three-cluster model, always vanishes regardless of the wave function of ^{9}Li. This is most easily understood by acting the Hermitian conjugate of the GT operator on the ^{9}Be wave function and by noting that the spin-isospin part of the α-particle wave function is fully occupied.

The above discussion indicates that the simple three-cluster model for ^{9}Be must be modified to explain the β decay in spite of the successful results obtained in the previous subsections. The modification must be small enough not to destroy the agreement between experiment and the three-cluster model calculation. One possible way for the modification is to introduce the distortion of the α-particle into $t+p$ and $h+n$ configurations. To explore the consequence of this modification, let us assume that the intrinsic wave function of the α-particle can be expressed by

$$\phi_\alpha = \sqrt{1-c^2}\,\phi_\alpha^{(0)} + c\phi_\alpha^{(\mathrm{e})}, \tag{22}$$

where $\phi_\alpha^{(0)}$ represents the part which can be described by the 0s harmonic-oscillator Slater determinant, while $\phi_\alpha^{(\mathrm{e})}$ the distorted part which is orthogonal to $\phi_\alpha^{(0)}$. The ^{9}Be wave function in a more realistic three-cluster model can therefore be approximated by

$$|\Psi_{J_f}(^9\mathrm{Be})\rangle = \mathcal{N}\left\{(1-c^2)|\Psi_{J_f}^{(0)}(^9\mathrm{Be})\rangle + 2c\sqrt{1-c^2}|\phi_\alpha^{(0)}\phi_\alpha^{(\mathrm{e})}n\rangle + c^2|\phi_\alpha^{(\mathrm{e})}\phi_\alpha^{(\mathrm{e})}n\rangle\right\}. \tag{23}$$

Here the normalization constant, $\mathcal{N}$, is close to unity when c is small and it is suppressed below. The first term, $|\Psi_{J_f}^{(0)}(^9\mathrm{Be})\rangle = |\phi_\alpha^{(0)}\phi_\alpha^{(0)}n\rangle$, is nothing but the one described by the $\alpha+\alpha+n$ model and has no contribution to the β decay. By neglecting the last term, the GT matrix element is given by

$$\begin{aligned} M_{GT}(i \to f) &= 2c\sqrt{1-c^2}\Big\langle \phi_\alpha^{(0)}\phi_\alpha^{(\mathrm{e})}n \,\Big\|\, \sum_{k=1}^{9} t_-(k)\boldsymbol{\sigma}(k) \,\Big\|\, \Psi_{J_i}(^9\mathrm{Li}) \Big\rangle \\ &= 2\langle \Psi_{J_f}^{(0)}(^9\mathrm{Be})|\Psi'_{J_f}(^9\mathrm{Be})\rangle \Big\langle \Psi'_{J_f}(^9\mathrm{Be}) \,\Big\|\, \sum_{k=1}^{9} t_-(k)\boldsymbol{\sigma}(k) \,\Big\|\, \Psi_{J_i}(^9\mathrm{Li}) \Big\rangle \end{aligned} \tag{24}$$

with

$$|\Psi'_{J_f}(^9\mathrm{Be})\rangle = \sqrt{1-c^2}|\Psi_{J_f}^{(0)}(^9\mathrm{Be})\rangle + c|\phi_\alpha^{(0)}\phi_\alpha^{(\mathrm{e})}n\rangle. \tag{25}$$

Equations (24) and (25) are our basic equations to calculate the β decay matrix element when the distortion of the α-particle is included.

The wave function of eq. (25) is obtained by extending the three-cluster model to the four-cluster model which includes $\alpha+t+p+n$ and $\alpha+h+n+n$ partitions. In order to avoid excessive numerical calculations, the angular momentum channels and the cluster arrangements are rather limited. See Fig. 1(b) and Table IV. The spins of all the clusters

were coupled to $S = \frac{1}{2}$. The isospins were not coupled to a definite value so that the wave function of the extended model may in general contain the total isospin of $T = \frac{1}{2}$ and $\frac{3}{2}$. The potential favors $T = \frac{1}{2}$ for the low-lying states of ^{9}Be.

The intrinsic wave function of the t- and h-cluster was described by 0s harmonic-oscillator Slater determinant of the same size parameter ν as that of the α-particle. The ground state wave function obtained in the four-cluster model using the Minnesota potential of u=0.94 has the overlap integral of 0.971 with the one obtained in the three-cluster model. Therefore, this new wave function should yield substantially the same results as the previous one for the electromagnetic properties. This is just what we have expected to maintain in extending the model space.

To calculate the β-decay probability we use the ^{9}Li ground-state wave function which was obtained in a microscopic $\alpha + t + n + n$ four-cluster model [22]. This model for ^{9}Li reproduced both magnetic and quadrupole moments of the ground state very well. To fit the energy of the ^{9}Be ground state to its experimental value from the four-body threshold, we changed the u parameter to 0.88 in the four-cluster model calculation. The overlap integral of the wave functions between the three-cluster and four-cluster models becomes 0.973 and the resulting logft value is 5.60. The logft value is still a little too large compared to the experimental value of 5.31, but this calculation strongly indicates that we are on the right track. A further refined four-cluster model calculation for both ^{9}Be and ^{9}Li will reduce the disagreement between experiment and theory because such a calculation is expected to enhance the GT matrix element. The shell-model calculation [49] gives the logft value in the range of 4.86 to 5.64, depending on the interaction used. It is interesting to analyze in the way presented above the β decay of ^{9}C to the low-lying states of ^{9}B and an asymmetry in the β-decay matrix elements of $A = 9$ nuclei [49,19].

IV. SUMMARY

The microscopic multicluster model was applied to the study of the mirror nuclei ^{9}Be and ^{9}B. They were described in a three-cluster model comprising two α-particles and a single nucleon. The two-nucleon interaction consists of the central and spin-orbit potentials together with the Coulomb potential. The same two-nucleon potential was employed for both ^{9}Be and ^{9}B. The ground state of ^{9}Be, an only particle-bound state in this study, was obtained with the stochastic variational method, while the other particle-unbound states were studied by the complex scaling and the stabilization methods. The three-body dynamics of the clusters was taken into account by including both of the arrangements, $(\alpha\alpha)N$ and $(\alpha N)\alpha$, and by using relevant partial waves between the relative motion of the clusters. The calculated spectrum of ^{9}Be below an excitation energy of 8 MeV was in fair agreement with experiment. We obtained two broad overlapping resonances with $J^\pi = \frac{7}{2}^-$ and $\frac{9}{2}^+$ around 6.5 MeV, in agreement with the conclusion of the recent experiments. Two states, $\frac{3}{2}^-_2$ and $\frac{5}{2}^-_2$, were predicted at about 4.5 MeV and 8MeV in excitation energy, respectively. The spectrum of ^{9}B was found to be similar to that of ^{9}Be. The spin and parity of several states of ^{9}B were predicted. The first excited $\frac{1}{2}^+$ state was not localized in the present study and thus no definite argument was possible on a Thomas-Ehrman shift in this case.

The theory reproduced very well the electromagnetic properties of the ^{9}Be ground state

such as the charge radius, the magnetic moment, the quadrupole moment, and the elastic electron scattering form factors. The calculated ground state density was consistent with the total reaction cross section data. The intrinsic deformation parameter of the density was found to be 0.89. The $\frac{1}{2}^+ \rightarrow \frac{3}{2}^-$ $E1$ transition and the $\frac{5}{2}^- \rightarrow \frac{3}{2}^-$ $E2/M1$ transitions were studied by treating the excited states as bound. The calculated transition rates were in good agreement with experiment.

The fact that the present calculation reproduced all the data well strongly supports that the three-cluster model is quite appropriate for describing the structure of ^{9}Be and ^{9}B, provided a full account of the dynamics is taken into account in the calculation. We were also able to understand the β decay of ^{9}Li to ^{9}Be by admixing the small components that are induced by the distortion of the α-particle into $t + p$ and $h + n$ configurations. A unique advantage of the microscopic multicluster model was exemplified by being able to accommodate such distortion in the model consistently. The study on heavier Be isotopes is in progress in the framework of the microscopic multicluster model including two α-particles and several neutrons.

This work was supported by a Grant-in Aid for Scientific Research (No. 05243102 and No. 0664038) of the Ministry of Education, Science and Culture (Japan) and by OTKA Grant No. T17298 (Hungary). Most of the calculations were done with the use of RIKEN's VPP500 computer.

REFERENCES

[1] I. Tanihata, H. Hamagaki, O. Hashimoto, Y. Shida, N. Yoshikawa, K. Sugimoto, O. Yamakawa, T. Kobayashi, and N. Takahashi, Phys. Rev. Lett. **55**, 2676 (1985); I. Tanihata, T. Kobayashi, O. Yamakawa, S. Shimoura, K. Ekuni, K. Sugimoto, N. Takahashi, T. Shimoda, and H. Sato, Phys. Lett. B **206**, 592 (1988).

[2] Y. Suzuki, Proc. of sixth Int. Conf. on Clusters in Nuclear Structure and Dynamics, edited by F. Haas, (Strasbourg, 1994), p.145; Y. Suzuki, K. Arai, Y. Ohbayasi, and K. Varga, Nucl. Phys. **A588**, 15c (1995).

[3] K. Langanke, in *Advances in Nuclear Physics*, vol. **21**, edited by J. W. Negele and E. Vogt, (Plenum, New York, 1994), p.85.

[4] D. Baye, Proc. of sixth Int. Conf. on Clusters in Nuclear Structure and Dynamics, edited by F. Haas, (Strasbourg, 1994), p.259; D. Baye, P. Descouvemont, and N. K. Timofeyuk, Nucl. Phys. **A588**, 147c (1995).

[5] J. P. Glickman *et al.*, Phys. Rev. C **43**, 1740 (1991).

[6] S. Dixit *et al.*, Phys. Rev. C **43**, 1758 (1991).

[7] F. Ajzenberg-Selove, Nucl. Phys. **A490**, 1 (1988).

[8] M. Bouten, M.-C. Bouten, H. Depuydt, and L. Schotsmans, Nucl. Phys. **A127**, 177 (1969).

[9] A. G. M. van Hees and P. W. M. Glaudemans, Z. Phys. A− Atoms and Nuclei **315**, 223 (1984); A. G. M. van Hees, A. A. Wolters, and P. W. M. Glaudemans, Nucl. Phys. **A476**, 61 (1988).

[10] A. C. Fonseca, J. Revai and A. Matveenko, Nucl. Phys. **A326**, 182 (1979); J. Revai and A. V. Matveenko, *ibid.* **A339**, 448 (1980).

[11] M. C. Orlowski, Bao Cheng-guang, and Liu-yuen, Z. Phys. A− Atoms and Nuclei **305**, 249 (1982).

[12] V. T. Voronchev, V. I. Kukulin, V. N. Pomerantsev, Kh. D. Razikov, and G. G. Ryzhikh, Yad. Fiz. **57**, 1964 (1994).

[13] W. Zahn, Nucl. Phys. **A269**, 138 (1976).

[14] S. Okabe, Y. Abe, and H. Tanaka, Prog. Theor. Phys. **57**, 866 (1977); S. Okabe and Y. Abe, *ibid.* **59**, 315 (1978); *ibid.* **61**, 1049 (1979).

[15] H. Furutani, H. Kanada, T. Kaneko, S. Nagata, H. Nishioka, S. Okabe, S. Saito, T. Sakuda, and M. Seya, Prog. Theor. Phys. Suppl. **68**, 193 (1980).

[16] P. Descouvemont, Phys. Rev. C**39**, 1557 (1989).

[17] D. J. Millener, J. W. Olness, E. K. Warburton, and S. S. Hanna, Phys. Rev. C**28**, 497 (1983).

[18] F. C. Barker, Aust. J. Phys. **37**, 267 (1984).

[19] G. Nyman *et al.*, Nucl. Phys. **A510**, 189 (1990).

[20] R. Sherr and G. Bertsch, Phys. Rev. C**32**, 1809 (1985).

[21] M. A. Tiede *et al.*, Phys. Rev. C**52**, 1315 (1995).

[22] K. Varga, Y. Suzuki, and I. Tanihata, Phys. Rev. C**52**, 3013 (1995).

[23] K. Varga and Y. Suzuki, Phys. Rev. C**52**, 2885 (1995).

[24] V. I. Kukulin and V. M. Krasnopol'sky, J. Phys. G **3** 795 (1977).

[25] K. Varga, Y. Suzuki, and R. G. Lovas, Nucl. Phys. **A571**, 447 (1994).

[26] K. Varga, Y. Suzuki, and Y. Ohbayasi, Phys. Rev. C **50**, 189 (1994).

[27] J. Aguilar and J. M. Combes, Commun. math. Phys. **22**, 269 (1971); E. Balslev and J. M. Combes, *ibid.* **22**, 280 (1971); B. Simon, *ibid.* **27**, 1 (1972).
[28] A. U. Hazi and H. S. Taylor, Phys. Rev. A **1**, 1109 (1970); C. H. Maier, L. S. Cederbaum, and W. Domcke, J. Phys. B: Atom. Molec. Phys. **13**, L119 (1980); V. A. Mandelshtam, H. S. Taylor, V. Ryaboy, and N. Moiseyev, Phys. Rev. A **50**, 2764 (1994), and references therein.
[29] A. T. Kruppa, R. G. Lovas, and B. Gyarmati, Phys. Rev. C **37**, 383 (1988); A. T. Kruppa and K. Kato, Prog. Theor. Phys. **84**, 1145 (1990).
[30] A. Csótó, Phys. Rev. C **49**, 2244 (1994); S. Aoyama, S. Mukai, K. Kato, and K. Ikeda, Prog. Theor. Phys. **93**, 99 (1995).
[31] D. R. Thompson, M. Lemere, and Y. C. Tang, Nucl. Phys. **A286**, 53 (1977); I. Reichstein and Y. C. Tang, *ibid.* **A158**, 529 (1970).
[32] B. Pugh, quoted in [21].
[33] R. G. Thomas, Phys. Rev. **88**, 1109 (1952); J. B. Ehrman, Phys. Rev. **81**, 412 (1951).
[34] S. Cohen and D. Kurath, Nucl. Phys. **73**, 1 (1965).
[35] T. de Forest and J. D. Walecka, Adv. Phys. **15**, 1 (1966).
[36] U. Meyer-Berkhout, K. W. Ford, and A. E. S. Green, Ann. Phys. **8**, 119 (1959).
[37] M. Bernheim, T. Stovall, and D. Vinciguerra, Nucl. Phys. **A97**, 488 (1967); M. Bernheim, R. Riskalla, T. Stovall, and D. Vinciguerra, Phys. Lett. **30B**, 412 (1969).
[38] A. G. Slight, T. E. Drake, and G. R. Bishop, Nucl. Phys. **A208**, 157 (1973).
[39] T. Janssens, R. Hofstadter, E. B. Hughes, and M. R. Yearian, Phys. Rev. **142**, 922 (1966).
[40] R. E. Rand, R. Frosch, and M. R. Yearian, Phys. Rev. **144**, 859 (1966).
[41] L. Lapikás, G. Box, and H. de Vries, Nucl. Phys. **A253**, 324 (1975).
[42] A. Bohr and B. Mottelson, *Nuclear Structure* (Benjamin, New York, 1975), Vol. II.
[43] S. Raman, C. H. Malarkey, W. T. Milner, C. W. Nestor, Jr., and P. H. Stelson, Atomic Data and Nuclear Data Tables **36**, 1 (1987).
[44] R. J. Glauber, Lectures in Theoretical Physics (Interscience, New York, 1959), Vol. 1, p. 315.
[45] Y. Ogawa, K. Yabana and Y. Suzuki, Nucl. Phys. **A543**, 722 (1922).
[46] M. G. Saint-Laurent *et al.*, Z. Phys. A−Atomic Nuclei **332**, 457 (1989).
[47] S. Kox *et al.*, Phys. Rev. C**35**, 1678 (1987).
[48] S. Saito, Prog. Theor. Phys. **41**, 705 (1969).
[49] D. Mikolas *et al.*, Phys. Rev. C**37**, 766 (1988).

TABLES

TABLE I. A set of arrangements and angular momenta included in the three-cluster model calculation for ^{9}Be ($N = n$) and ^{9}B ($N = p$). See Fig. 1(a) for the angular momenta ℓ_1 and ℓ_2.

J^π	arrangement	angular momentum $(\ell_1, \ell_2)L$					
$1/2^-$	$(\alpha\alpha)N$	(0,1)1	(2,1)1	(2,3)1			
	$(\alpha N)\alpha$	(1,0)1	(1,2)1				
$1/2^+$	$(\alpha\alpha)N$	(0,0)0	(2,2)0	(2,2)1			
	$(\alpha N)\alpha$	(1,1)0	(1,1)1				
$3/2^-$	$(\alpha\alpha)N$	(0,1)1	(2,1)1	(2,1)2			
	$(\alpha N)\alpha$	(0,1)1	(1,0)1	(2,1)1	(1,2)1	(2,1)2	(1,2)2
$3/2^+$	$(\alpha\alpha)N$	(2,2)1	(0,2)2	(2,0)2	(2,2)2	(2,4)2	(4,2)2
	$(\alpha N)\alpha$	(1,1)1	(1,1)2	(1,3)2			
$5/2^-$	$(\alpha\alpha)N$	(2,1)2	(2,3)2	(0,3)3	(2,1)3	(2,3)3	
	$(\alpha N)\alpha$	(1,2)2	(1,2)3				
$5/2^+$	$(\alpha\alpha)N$	(0,2)2	(2,0)2	(2,2)2	(2,2)3		
	$(\alpha N)\alpha$	(1,1)2	(1,3)2	(1,3)3			
$7/2^-$	$(\alpha\alpha)N$	(2,1)3	(0,3)3	(2,3)3	(4,1)3	(2,3)4	(4,1)4
	$(\alpha N)\alpha$	(1,2)3	(1,4)3	(1,4)4			
$9/2^+$	$(\alpha\alpha)N$	(2,2)4	(0,4)4	(4,0)4	(2,4)4	(4,2)4	(4,4)4
		(2,4)5	(4,2)5	(4,4)5			
	$(\alpha N)\alpha$	(1,3)4	(1,5)4	(1,5)5			

TABLE II. Energies and widths of the unbound states in ^{9}Be and ^{9}B. The energy is from the three-body threshold. The spin and parity of the 3.065 MeV state of ^{9}B is assumed to be $\frac{5}{2}^+$.

		exp.[a]		cal.	
	J^π	E(MeV±keV)	Γ(MeV±keV)	E(MeV)	Γ(MeV)
^{9}Be	$3/2^-$	-1.5735	——-	-1.431	——-
	$1/2^+$	0.111±7	0.217±10		
	$5/2^-$	0.8559±1.3	0.00077±0.15	0.84	0.001
	$1/2^-$	1.21±120	1.080±110	1.20	0.46
	$5/2^+$	1.476±9	0.282±11	1.98	0.6
	$3/2^+$	3.131±25	0.743±55	3.3	1.6
	$3/2^-_2$	4.02±100[b]	1.33±360	2.9	0.8
	$7/2^-$	4.81±60[b]	1.21±230	5.03	1.2
	$9/2^+$	5.19±60[b]	1.33±90	4.9	2.9
	$(1/2^-)$	6.37±80	∼1.0		
	$5/2^-_2$			6.5	2.1
^{9}B	$3/2^-$	0.277	0.00054±0.21	0.30	0.004
	$1/2^+$	(1.9)	≃0.7		
	$5/2^-$	2.638±5	0.081±5	2.55	0.044
	$1/2^-$	3.11[c]	3.1	2.73	1.0
	$5/2^+$	3.065±30	0.550±40	3.5	1.2
	$3/2^+$			4.6	2.7
	$3/2^-_2$			4.2	1.4
	$7/2^-$	7.25±60	2.0±200	7.0	1.7
	$9/2^+$			6.6	3.3
	$5/2^-_2$			8.4	2.4

a) Ref. [7]. b) Ref. [6]. c) Ref. [32].

TABLE III. Radii and electromagnetic properties of ^{9}Be. The reduced matrix elements are given in Weisskopf units. The bare-nucleon charges and g-factors are used in the present calculation. The effective charges were used in the shell model calculation of Refs. [5] and [9] to calculate the quadrupole moment and the $E2$ strength. See text for the $B(E1)$ value of the present calculation.

J^π		exp.[a]	present	Ref. [15]	Ref. [16]	Ref. [5]	Ref. [9]
$3/2^-$	E (MeV)	-1.5735	-1.431		-0.89		
	r_m (fm)		2.50	2.62			
	r_p (fm)	2.37±0.01	2.39				
	r_n (fm)		2.58				
	μ (μ_N)	-1.1778±0.0009	-1.169	-1.23	-1.52	-1.27	-1.070
	Q (e fm^2)	5.3±0.3	5.13	5.76	4.77	4.35	4.66
	σ_R (mb)	825±20 [b]	850				
$5/2^-$	E (MeV)	0.8559	0.883		1.89		
	$B(E2; \frac{5}{2}^- \to \frac{3}{2}^-)$	24.4±1.8	22.0	24.7	23.5	12.5	~ 7
	$B(M1; \frac{5}{2}^- \to \frac{3}{2}^-)$	0.30±0.03	0.229		0.10	0.23	
$1/2^+$	E (MeV)	0.111			0.05		0.75
	$B(E1; \frac{1}{2}^+ \to \frac{3}{2}^-)$	0.22±0.09	0.24		0.68	0.03	0.03
			0.18				

a) Ref. [7]. b) Ref. [46].

TABLE IV. A set of arrangements and angular momenta included in the four-cluster model calculation for the ^{9}Be ground state. See Fig. 1(b) for the angular momenta ℓ_1, ℓ_2, and ℓ_3. The spin of the nucleon clusters is coupled to s_{23}. The total spin S is restricted to $\frac{1}{2}$.

J^π	arrangement	angular momentum $[(\ell_1,\ell_2)\ell_{12},\ell_3]L$			s_{23}
^{9}Be: $3/2^-$	$((tp)\alpha)n$	[(0,0)0,1]1	[(0,2)2,1]1	[(0,2)2,1]2	1
	$(tp)(\alpha n)$	[(0,0)0,1]1	[(0,2)2,1]1	[(0,2)2,1]2	1
	$((tp)n)\alpha$	[(0,1)1,0]1	[(0,1)1,2]1	[(0,1)1,2]2	1
	$((tn)\alpha)p$	[(0,0)0,1]1	[(0,2)2,1]1	[(0,2)2,1]2	1
	$(tn)(\alpha p)$	[(0,0)0,1]1	[(0,2)2,1]1	[(0,2)2,1]2	1
	$((tn)p)\alpha$	[(0,1)1,0]1	[(0,1)1,2]1	[(0,1)1,2]2	1
	$((hn)\alpha)n$	[(0,0)0,1]1	[(0,2)2,1]1	[(0,2)2,1]2	0
	$(hn)(\alpha n)$	[(0,0)0,1]1	[(0,2)2,1]1	[(0,2)2,1]2	0
	$((hn)n)\alpha$	[(0,1)1,0]1	[(0,1)1,2]1	[(0,1)1,2]2	0

Figure Captions

Fig. 1. Different arrangements used in the three-body (a) and four-body (b) calculations. The small circles are nucleons, the medium-size circle is α-particle, and the gray circle is $3N$-cluster, t or h. The orbital angular momenta for the relative motion between the clusters connected by solid lines are denoted by ℓ_i. The spin of the clusters is $s_i = \frac{1}{2}$; the spin of the α-particle is zero and it is omitted.

Fig. 2. Complex eigenvalues for $J^\pi = \frac{3}{2}^-$ (a) and $\frac{7}{2}^-$ (b) of ^{9}Be. The rotation angle θ is in units of radian. The point indicated by an open circle corresponds to a resonance.

Fig. 3. Experimental and calculated energies of ^{9}Be (a) and ^{9}B (b) from the three-body threshold. The data are from Refs. [5,6,7]. The 3.065 MeV state of ^{9}B is assumed to be $\frac{5}{2}^+$.

Fig. 4. Elastic charge form factor for ^{9}Be. The data are from Refs. [36,37,38].

Fig. 5. Elastic transverse form factor for ^{9}Be. The data are from Refs. [40,41].

Fig. 6. Monopole (a) and quadrupole (b) density distributions of protons and neutrons for the ground state of ^{9}Be.

Fig. 7. Monopole density distributions of protons and neutrons, (a) in linear scale and (b) in logarithmic scale, for the excited $\frac{1}{2}^+$ state and the $\frac{3}{2}^-$ ground state of ^{9}Be. The value of $u = 1.0$ is used for the $\frac{1}{2}^+$ state.

Fig. 8. Spectroscopic amplitudes of the ground state of ^{9}Be for the ^{8}Be+n arrangement. The symbols r and R denote the distances of two α-particles and of n from their center-of-mass. The set of angular momenta is (a) $\ell_1 = 0, \ell_2 = 1, L = 1$, (b) $\ell_1 = 2, \ell_2 = 1, L = 1$, and (c) $\ell_1 = 2, \ell_2 = 1, L = 2$.

Fig. 9. Spectroscopic amplitudes of the ground state of ^{9}Be for the ^{5}He+α arrangement. The symbol r is the distance between n and α and R the distance between their center-of-mass and α. The set of angular momenta is (a) $\ell_1 = 1, \ell_2 = 0, L = 1$, (b) $\ell_1 = 1, \ell_2 = 2, L = 1$, and (c) $\ell_1 = 1, \ell_2 = 2, L = 2$.

(a) 3-body cluster arrangement

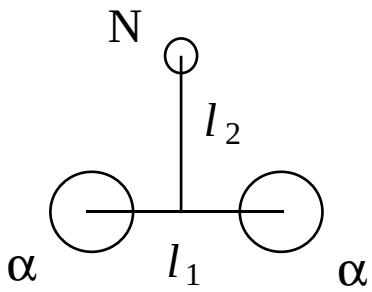

(α α)N

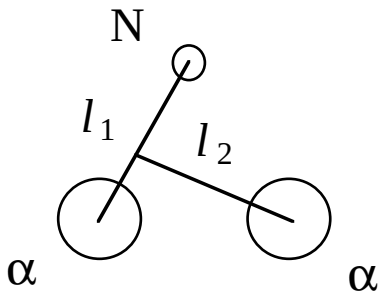

(α N)α

(b) 4-body cluster arrangement

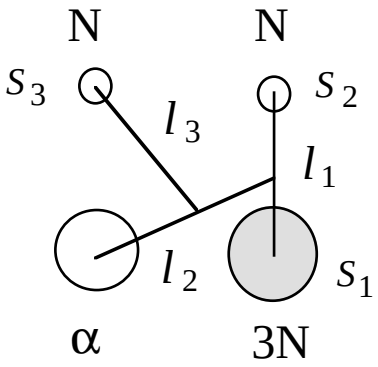

((3N, N) α))N

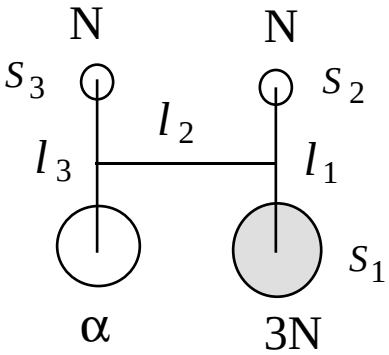

(3N, N) (α N)

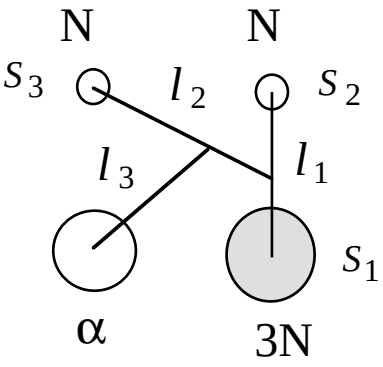

((3N, N)N)) α

Fig. 1

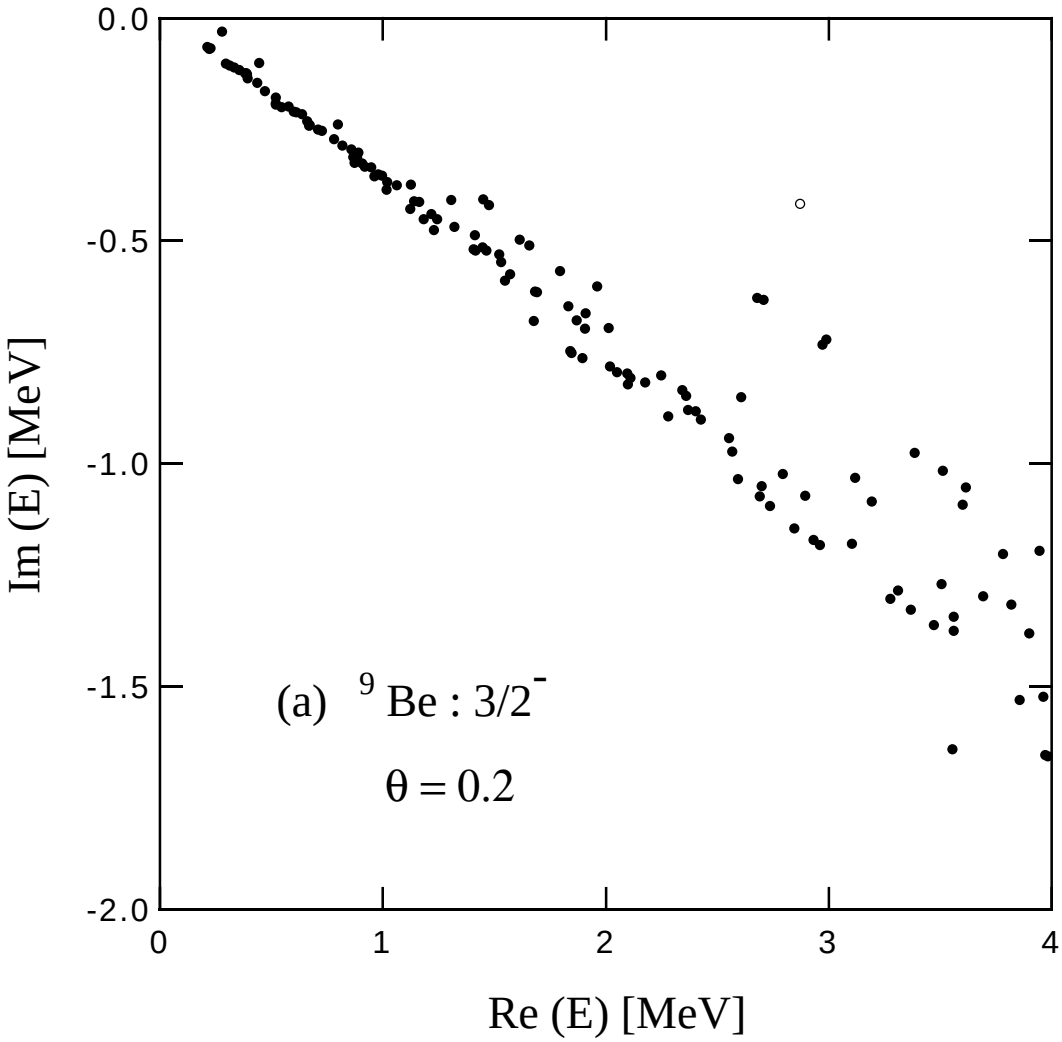

Fig. 2 (a)

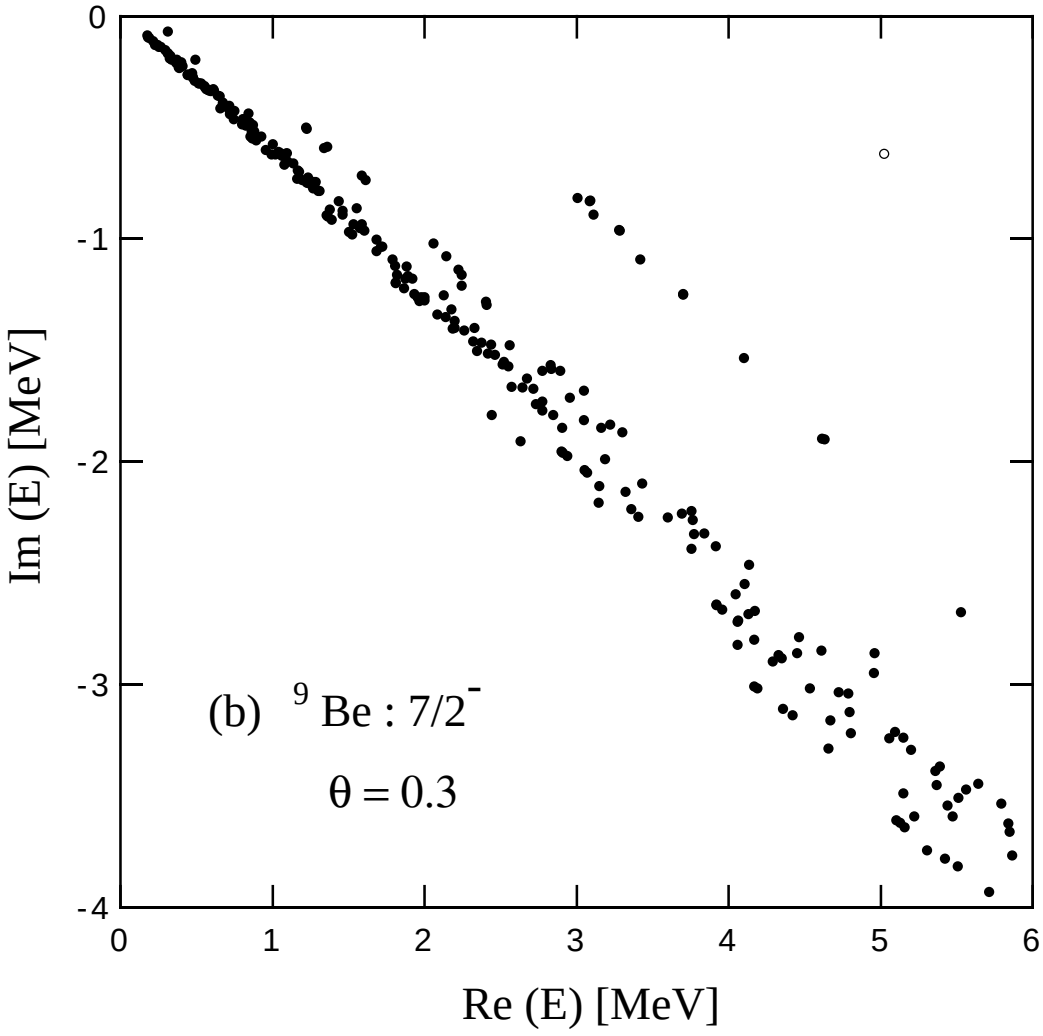

Fig. 2 (b)

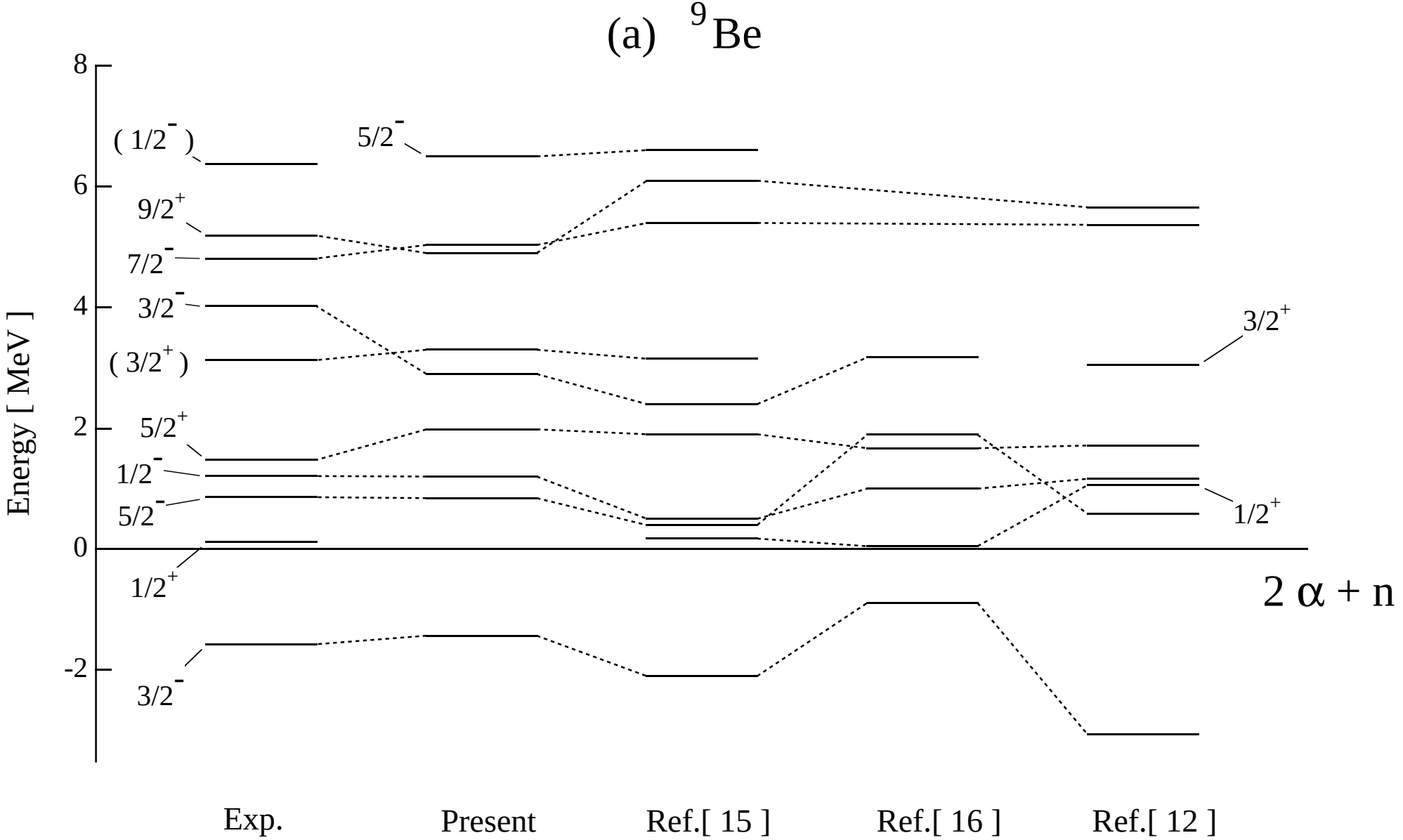
(a) 9Be
Energy [MeV]
8
6
4
2
0
-2
(1/2-)
5/2-
9/2+
7/2-
3/2-
(3/2+)
5/2+
1/2-
5/2-
1/2+
3/2-
3/2+
1/2+
2 α + n
Exp.
Present
Ref.[15]
Ref.[16]
Ref.[12]

Fig.3 (a)

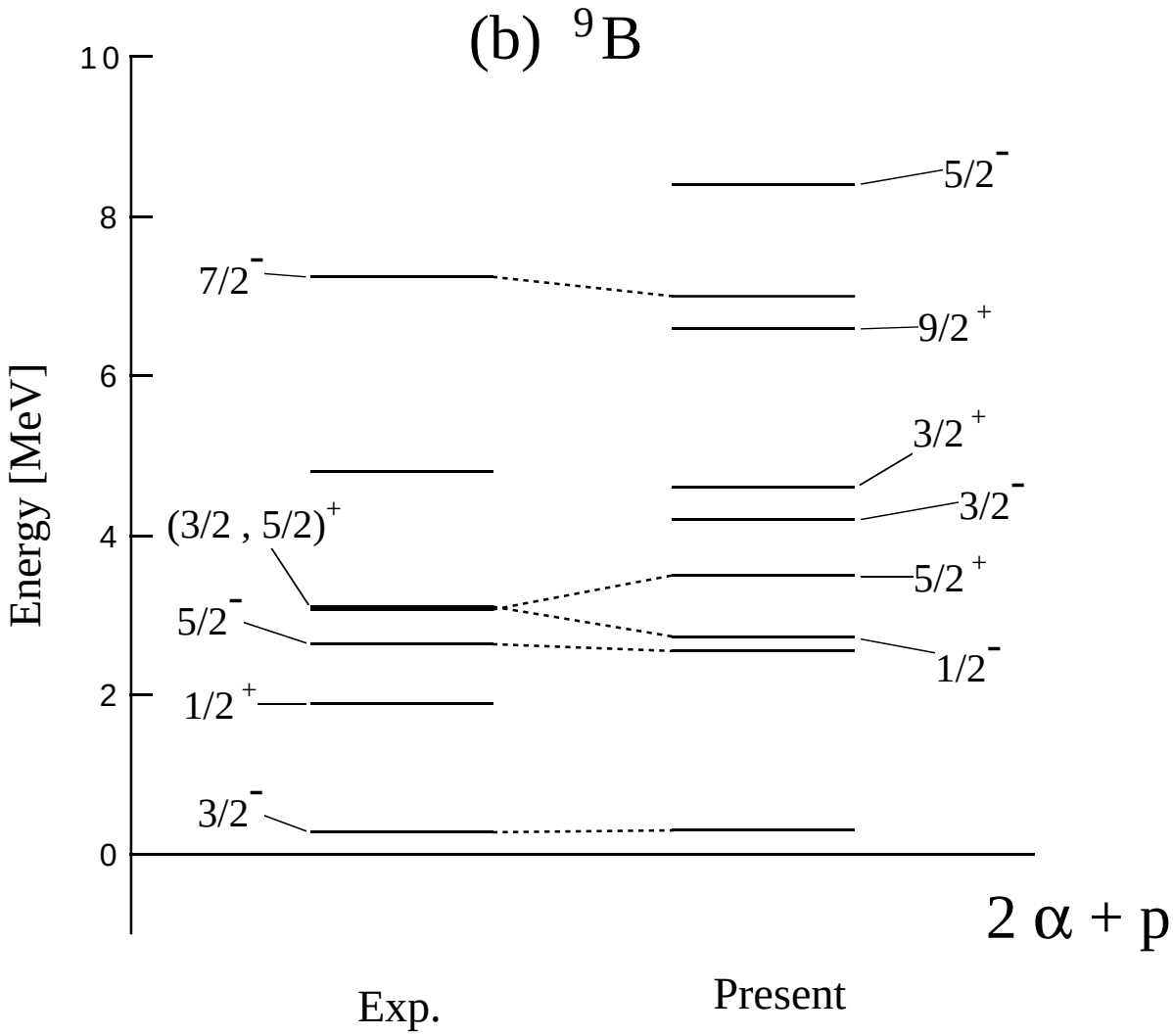
(b) ^{9}B
Energy [MeV]
10
8
6
4
2
0
7/2$^-$
(3/2 , 5/2)$^+$
5/2$^-$
1/2$^+$
3/2$^-$
5/2$^-$
9/2$^+$
3/2$^+$
3/2$^-$
5/2$^+$
1/2$^-$
2 α + p
Exp.
Present

Fig.3 (b)

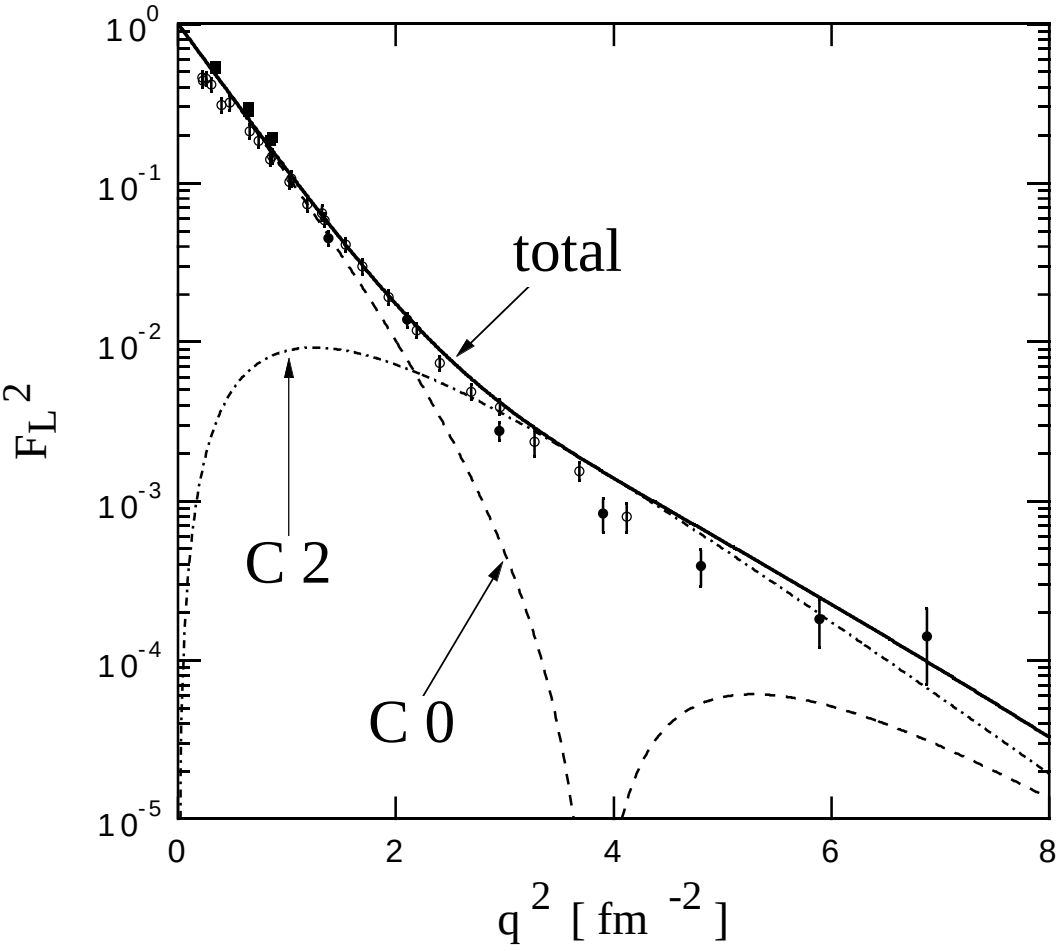

Fig.4

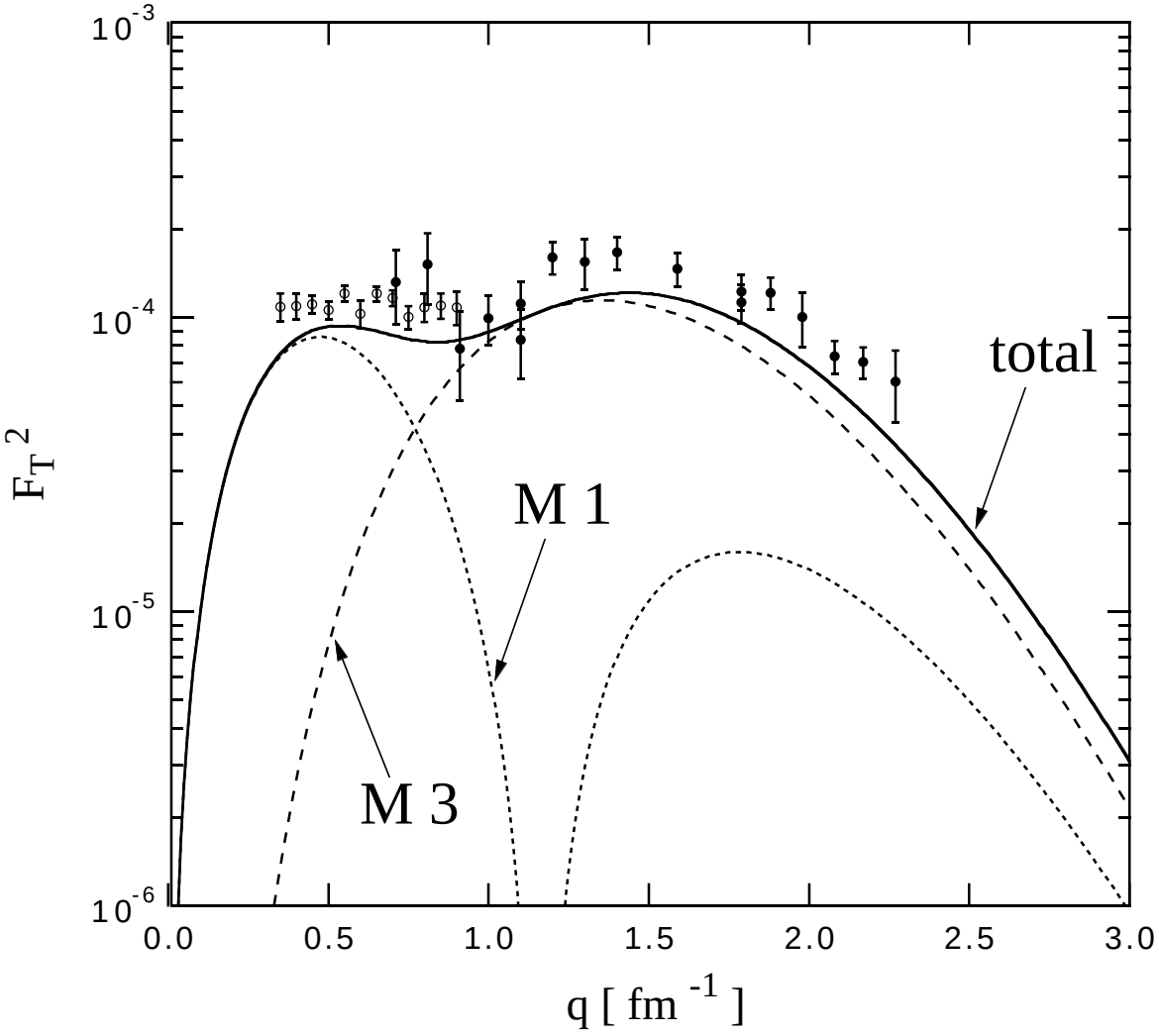

Fig.5

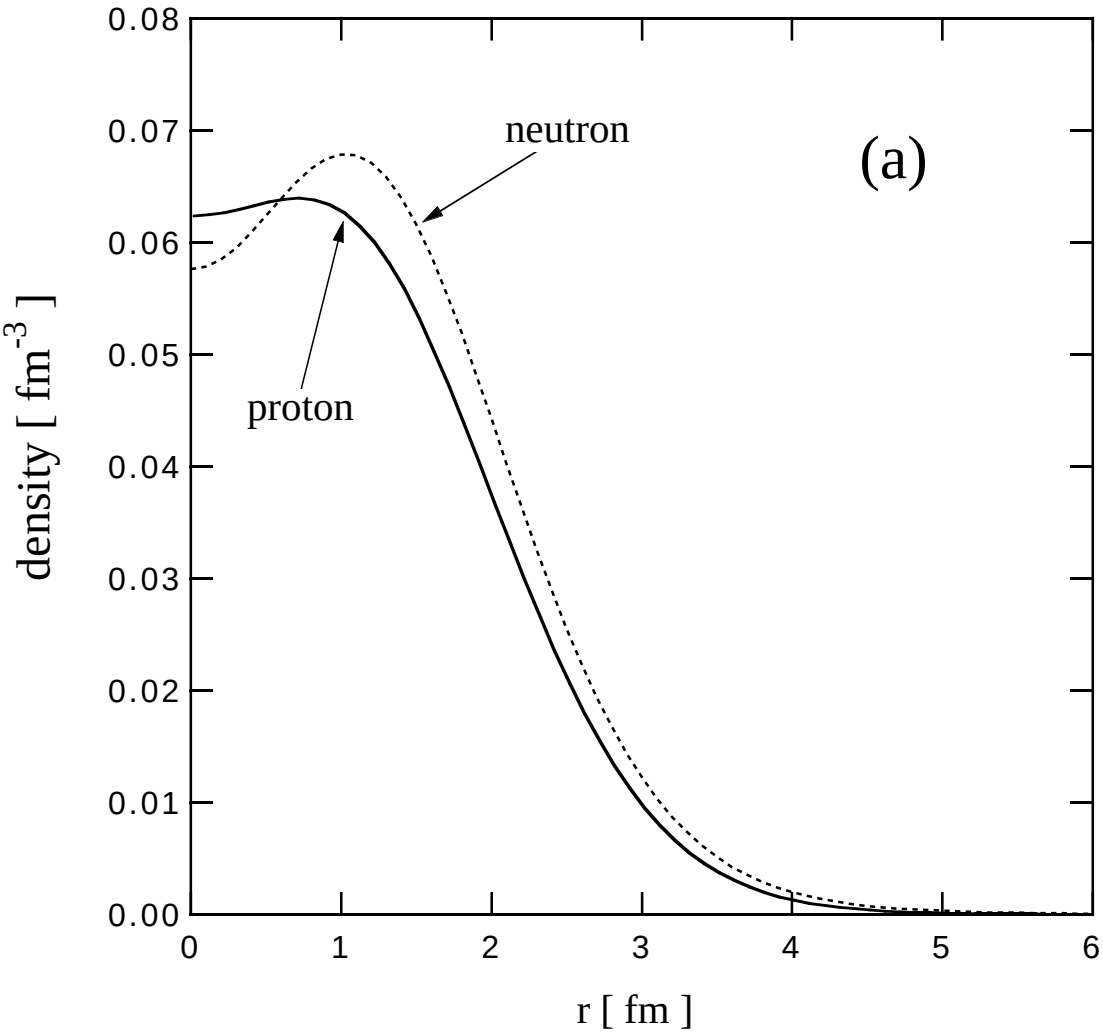
0.08
0.07
0.06
0.05
0.04
0.03
0.02
0.01
0.00
0
1
2
3
4
5
6
density [fm-3]
r [fm]
neutron
proton
(a)

Fig.6 (a)

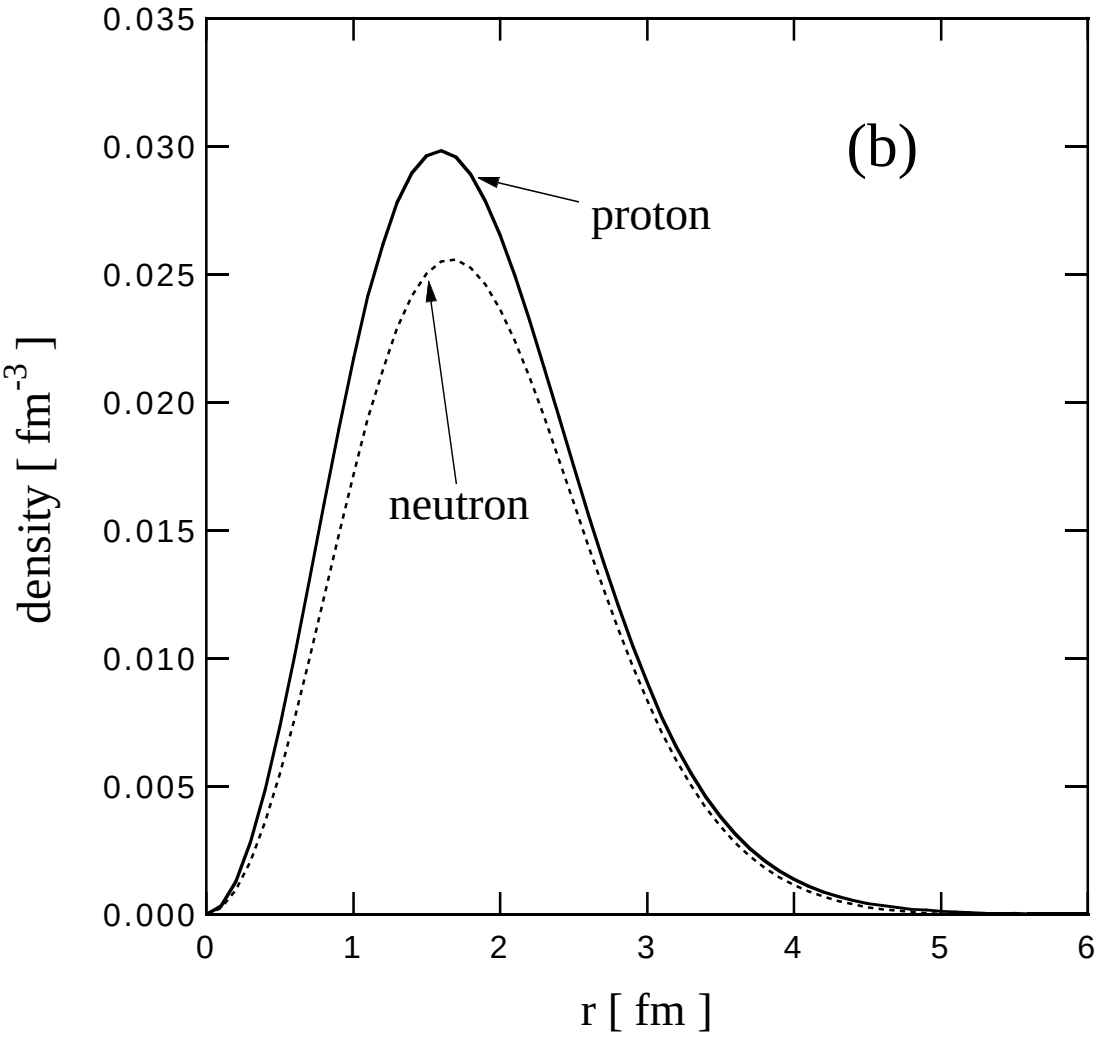
(b)
proton
neutron
density [fm^{-3}]
r [fm]
0.035
0.030
0.025
0.020
0.015
0.010
0.005
0.000
0
1
2
3
4
5
6

Fig.6 (b)

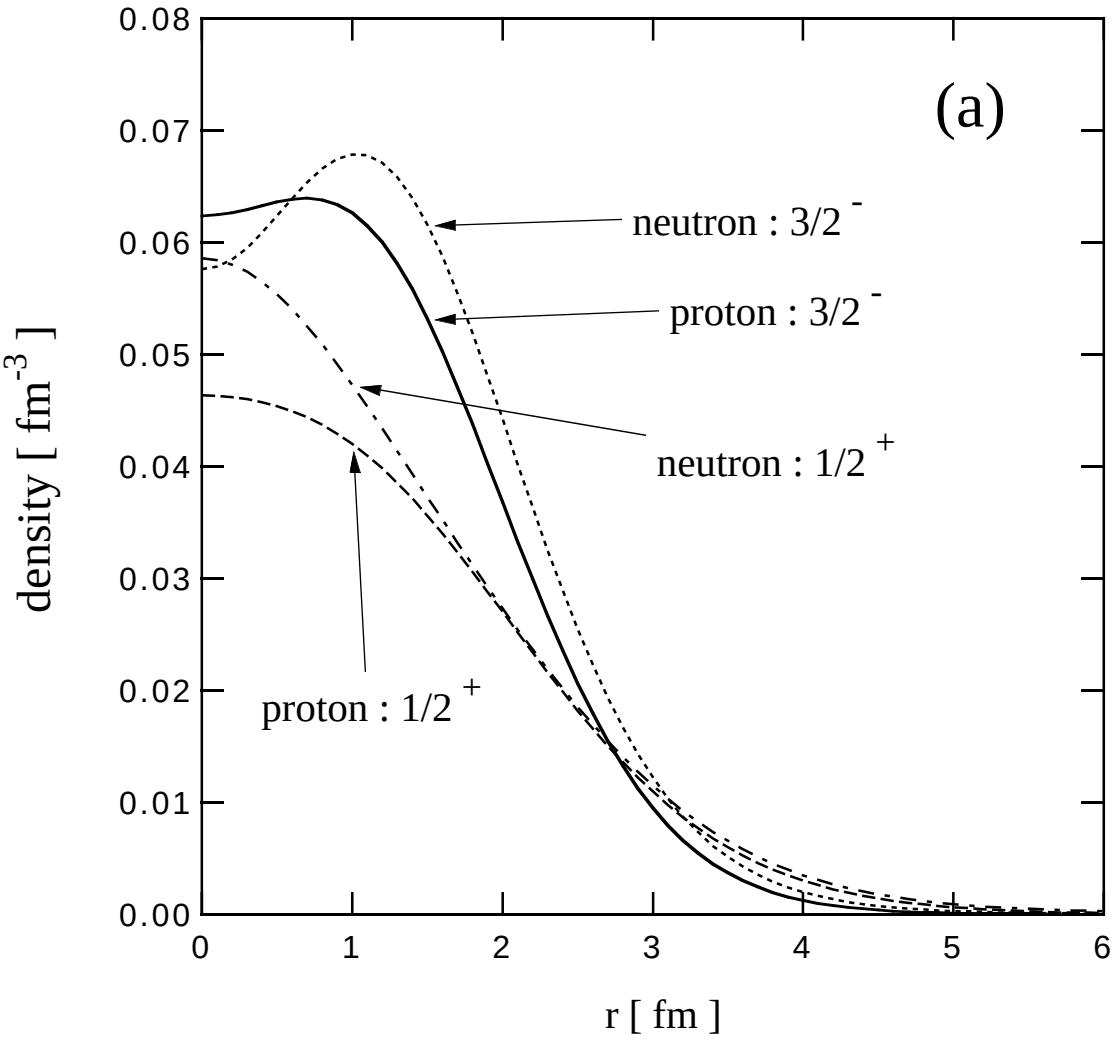
(a)
neutron : 3/2 -
proton : 3/2 -
neutron : 1/2 +
proton : 1/2 +
density [fm-3]
r [fm]
0.08
0.07
0.06
0.05
0.04
0.03
0.02
0.01
0.00
0
1
2
3
4
5
6

Fig. 7 (a)

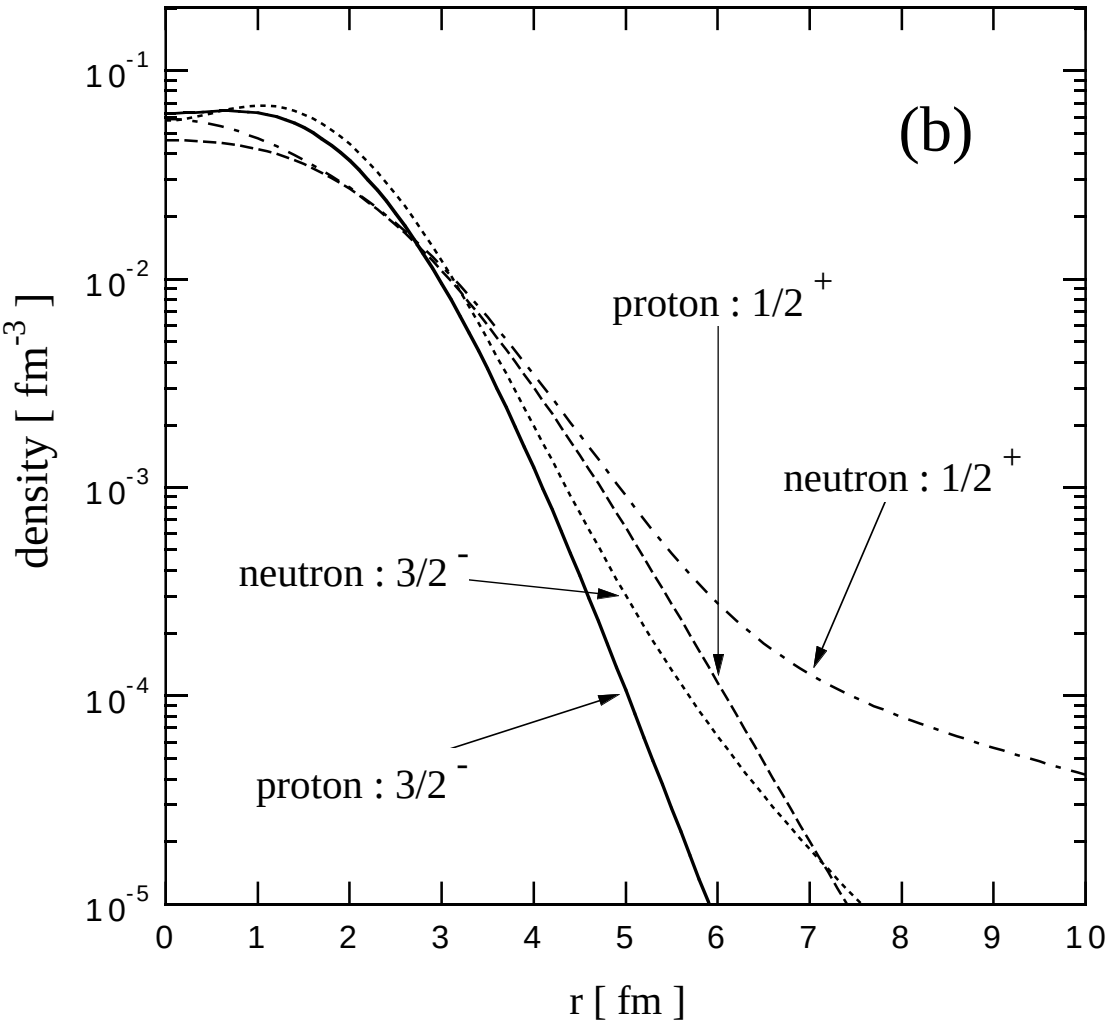
(b)
density [fm^{-3}]
r [fm]
proton : 1/2 $^{+}$
neutron : 1/2 $^{+}$
neutron : 3/2 $^{-}$
proton : 3/2 $^{-}$
10^{-1}
10^{-2}
10^{-3}
10^{-4}
10^{-5}
0
1
2
3
4
5
6
7
8
9
10

Fig. 7 (b)